https://doi.org/10.5194/se-2020-44
Preprint. Discussion started: 29 April 2020

Tectonic Exhumation of the Central Alps Recorded by Detrital Zircon in the Molasse Basin, Switzerland

Owen A. Anfinson[1,2], Daniel F. Stockli[2], Joseph C. Miller[3], Andreas Möller[3], Fritz Schlunegger[4]

[1]Sonoma State University, Department of Geology, Rohnert Park, CA, 94928
[2]University of Texas at Austin, Department of Geological Sciences, Jackson School of Geoscience, Austin, TX, 78712
[3]University of Kansas, Department of Geology, Lawrence, KS
[4]University of Bern, Institute of Geological Sciences, Bern, CH

Correspondence to: Owen A. Anfinson (anfinson@sonoma.edu)

https://doi.org/10.5194/se-2020-44
Preprint. Discussion started: 29 April 2020

Solid Earth Discussions Open Access EGU

Abstract

Eocene to Miocene sedimentary strata of the Northern Alpine Molasse Basin in Switzerland are well studied, yet they lack robust geochronologic and geochemical analysis of detrital zircon for provenance tracing purposes. Here, we present detrital zircon U-Pb ages coupled with rare earth and trace element geochemistry (petrochronology) to provide insights into the sedimentary provenance and to elucidate the tectonic activity of the central Alpine Orogen from the late Eocene to mid Miocene. Between 35-22.5 ± 1 Ma, the detrital zircon U-Pb age signatures were dominated by age groups of 300-370 Ma, 370-490 Ma, and 490-710 Ma, with minor Proterozoic age contributions. In contrast, from 21.5 ± 1 Ma to ~13.5 Ma (youngest preserved sediments), the detrital zircon U-Pb signatures were dominated by a 252-300 Ma age group, with a secondary abundance of the 370-490 Ma age group, and only minor contributions of the 490-710 Ma age group. The Eo-Oligocene provenance signatures are consistent with interpretations that initial basin deposition primarily recorded exhumation and erosion of the Austroalpine orogenic cover and minor contributions from underlying Penninic units, containing reworked detritus from Variscan, Caledonian, and Cadomian orogenic cycles. The dominant 252-300 age group from the younger Miocene deposits is associated with the exhumation of Variscan-aged crystalline rocks of upper-Penninic basement units. Noticeable is the lack of Alpine-aged detrital zircon in all samples with the exception of one late Eocene sample, which reflects Alpine volcanism associated with incipient continent-continent collision. In addition, the REE and trace element data from the detrital zircon, coupled with zircon morphology and U/Th ratios, point primarily igneous and rare metamorphic sources of zircon.

The observed change in detrital input from Austroalpine to Penninic provenance in the Molasse Basin at ~22 Ma appears to be correlated with the onset of synorogenic extension of the Central Alps. Synorogenic extension accommodated by slip along the Simplon fault zone promoted updoming and exhumation the Penninic crystalline core of the Alpine Orogen. The lack of Alpine detrital zircon U-Pb ages in all Oligo-Miocene strata also shows that the Molasse Basin drainage network was not accessing the prominent Alpine age intrusions and metamorphic complexes located in the southern portion of the Central Alps.

1 Introduction

https://doi.org/10.5194/se-2020-44
Preprint. Discussion started: 29 April 2020

Foreland basins archive the evolution of collisional mountain belts and can provide powerful insights into geodynamic processes operating in the adjacent mountain belt, as the stratigraphy of these basins directly record the history of subduction, thrusting and erosion in the adjacent orogen (Jordan and Flemings, 1991; Sinclair and Allen, 1992; DeCelles and Giles, 1996). The Northern Alpine Foreland Basin in Switzerland, also known as the Swiss Molasse Basin, has long been the site of extensive research and helped define fundamental concepts applicable to other flexural foreland basins. Research has focused on sedimentary architecture and facies relationships (Diem, 1986; Platt and Keller, 1992; Kempf et al., 1999; Garefalakis and Schlunegger, 2019), biostratigraphy (Engesser and Mayo, 1987; Schlunegger et al., 1996; Kälin and Kempf, 2009; Jost et al., 2016), and magnetostratigraphy (Schlunegger et al., 1996; Schlunegger et al., 1997a; Kempf et al., 1999; Strunck and Matter, 2002). These studies significantly refined the reconstruction of depositional processes within a detailed temporal framework (Kuhlemann and Kempf, 2002) and yielded a detailed picture of the basin evolution in response to orogenic processes (Sinclair and Allen, 1992; Allen et al., 2013; Schlunegger and Kissling, 2015). However, considerably less attention has been paid to exploring the origins of the sedimentary provenance. Available constraints from heavy mineral assemblages (Fuchtbauer, 1964; Gasser, 1966, 1968; Schlanke, 1974; Schlunegger et al., 1997a; Kempf et al., 1999) or clast suites of conglomerates (Habicht, 1945; Matter, 1964; Gasser, 1968; Stürm, 1973; Schlunegger et al., 1997a; Kempf et al., 1999) have largely been inconclusive in terms of sediment sourcing (Von Eynatten et al., 1999). Such insights, however, are of critical importance for reconstructing the causal relationships between orogenic events and the basinal stratigraphic response. In the recent years, advances in isotopic provenance tracing techniques, including detrital mica $^{40}Ar/^{39}Ar$ dating (e.g. Von Eynatten et al., 1999; Von Eynatten and Wijbrans, 2003), detrital garnet geochemical analysis (Stutenbecker et al., 2019), and detrital zircon U-Pb geochronology (e.g. Malusa et al., 2016; Anfinson et al., 2016; Lu et al., 2018; Sharman et al., 2018a) have offered more quantitative links to Alpine geodynamic processes, revealed through seismic tomography imaging (Lippitsch et al., 2003; Fry et al., 2010; Hetényi et al., 2018) or bedrock geochronology (Boston et al., 2017). In this study, we combine U-Pb ages with trace and rare earth element geochemistry of detrital zircon to elucidate the tectonic activity and unroofing history of the central Alpine orogen from the late-Eocene to mid-Miocene stratigraphic record of the Molasse Basin. We particularly focused on the Molasse deposits of the

https://doi.org/10.5194/se-2020-44
Preprint. Discussion started: 29 April 2020

Solid Earth Discussions

Lucerne area (Figure 1) due north of the Lepontine Dome, which is the largest and most prominent crystalline core in the central European Alps. We hypothesize that the fast tectonic unroofing/exhumation of the Penninic rocks in the core of the dome (Boston et al., 2017) resulted in a measurable signal within foreland basin sediments. For this purpose, we collected detrital zircon U-Pb data from Molasse sandstones near Lucerne (Figure 1) at a temporal resolution of 1-2 myrs. We augmented this dataset with detrital zircon U-Pb ages from a western section near Thun (Figure 1) and eastern section near Bregenz in Austria (Figure 1) at a lower temporal resolution to explore lateral provenance variations. This comprehensive new detrital zircon U-Pb dataset from the Northern Alpine Molasse Basin allows us to illuminate the orogenic hinterland erosional processes, syn-tectonic drainage evolution, and, linkages to the progressive tectonic unroofing in the Central Alps as well as the influence on the long-term stratigraphic development of the Swiss Molasse Basin.

2 The Central Alps: Architecture and Evolution

2.1 Architecture

The continental collision between Adria, a promontory of the African plate, and the European plate resulted in the Cenozoic Alpine orogen (Stampfli and Borel, 2002; Schmid et al., 2004). Convergence began with the subduction of European oceanic lithosphere beneath the Adriatic continental plate in the Late Cretaceous, resulting in the closure of the Alpine Tethys ocean (Schmid et al., 1996; Lihou and Allen, 1996) and culminating in the final continental collision, which started at ~35 Ma at the latest (Kissling and Schlunegger, 2018). This orogeny resulted in the construction of an ultimately bivergent orogen with the Periadriatic Lineament separating the Northern Alps from the Southern Alps (Schmid et al., 1989). The core of the north- and northwest-vergent Northern Alps is characterized by pervasive Alpine ductile deformation and metamorphism of the basement and associated cover units (Schmid et al., 2004). The south-vergent Southern Alps generally experienced thick- and thin-skinned deformation (Laubscher, 1983) with limited Alpine metamorphic overprinting.

The litho-tectonic units of the Northern Alps have been categorized into three broad nappe systems based on their paleogeographic position in Mesozoic times (Figure 1; Schmid et al., 2004; Spiegel et al., 2004). The Helvetic units along the northern margin of the orogen form a stack of thrust sheets that consist of Mesozoic limestones and marls. These sediments

https://doi.org/10.5194/se-2020-44
Preprint. Discussion started: 29 April 2020

accumulated on the stretched (Helvetic units) and distal rifted (Ultrahelvetic units) European continental margin during the Mesozoic phase of rifting and spreading (Schmid et al., 1996; Schmid et al., 2004). The basal thrust of the Helvetic nappes, referred to as the basal Alpine thrust (Figure 1), was folded in response to basement-involved shortening within the European plate at ~20 Ma, resulting in the uplift of the external massifs (Herwegh et al., 2017), exposing Variscan amphibolites and metagranites dated by U-Pb geochronology to 290 to 330 Ma (Schaltegger et al., 2003; von Raumer et al., 2009). The Penninic units represent the oceanic domains of the Piemont-Liguria and Valais basins, separated by the Brianconnais or Iberian microcontinent (Schmid et al., 1996). The Austroalpine units, both basement and sedimentary cover, formed the northern margin of the Adriatic plate (Pfiffner et al., 2002; Schmid et al., 2004; Handy et al., 2010). While there are few Austroalpine units preserved in the Western and Central Alps, where the exposed rocks belong mainly to the Helvetic and Penninic units, the Austroalpine rocks dominate the Eastern Alps forming an orogenic lid, with Penninic and Helvetic units only exposed in tectonic windows (Figure 1; Schmid et al., 2004). The Lepontine Dome forms the crystalline core of the Penninic nappes and mainly exposes moderate- to high-grade Variscan ortho- and paragneisses separated by Mesozoic metasedimentary slivers (Spicher, 1980). Along the western margin, the dome is bordered by the extensional Simplon shear zone and detachment fault (Mancktelow, 1985; Schmid et al., 1996), accommodating tectonic exhumation since ~30 Ma (Gebauer, 1999). Rates of synorogenic unroofing of the Lepontine dome appears to have peaked between 20-15 Ma (Grasemann and Mancktelow, 1993; Boston et al., 2017) as indicated by cooling ages imply, but potentially started prior to 20 Ma as suggested by Schlunegger and Willett (1999), considering a thermal lag time after the onset of faulting.

2.2 Pre-Alpine Tectonic Evolution

Since the Neoproterozoic at least three pre-Alpine orogenies contributed to the growth and reworking of the continental crust of the European, Iberian, and Adriatic plates that now make up the Alpine orogen (von Raumer, 1998; Schaltegger and Gebauer, 1999; Schaltegger et al., 2003). As it is important to understand these precursor orogenic events recorded by the detrital zircon data, these orogenic cycles are discussed below from oldest to youngest.

2.2.1 Cadomian Orogeny

The Cadomian orogeny has been interpreted as an Andean-style per-Gondwanan belt that resulted in accretion of island arc and continental margin strata along the Gondwanan continental margin from late Neoproterozoic to Cambrian times (von Raumer et al., 2002; Kröner and Stern, 2004). In general, the age range of this orogenic cycle is broadly considered to be 650 to 550 Ma; however, some consider the orogenic cycle to encompass a greater timespan of 700-480 Ma (D'Lemos et al., 1990). In the present Alpine orogen, recycled detritus related to the Cadomian orogeny is preserved in the basement units of the Gotthard Massif, Habach complex, and Austro-Alpine Silvretta nappe (Müller et al., 1996), as well as in the Mesozoic and Cenozoic strata of the Schlieren Flysch (Bütler et al., 2011). Cadomian zircon U-Pb crystallization ages preserved in both the sedimentary and basement units range from 650 to 600 Ma (Neubauer, 2002), while Cadomian magmatism lasted until at least 520 Ma (Neubauer, 2002). The Cadomian orogenic activity is also roughly synchronous to slightly younger compared to the Pan-African orogeny (Kröner and Stern, 2004).

2.2.2 Caledonian Orogeny

Evidence for Ordovician-aged Caledonian tectonism and magmatism are preserved in all of the major Alpine tectonic units (von Raumer, 1998; Engi et al., 2004). The Aar and Gotthard massifs of central Switzerland (Schaltegger et al., 2003), associated with the European continental lithosphere, as well the Austroalpine Silvretta nappe contain Caledonian granitoids (Schaltegger and Gebauer, 1999). In addition, sedimentary units, such as the Ultrahelvtic Flysch, also contain Ordovician detrital zircon grains (Bütler et al., 2011). Although felsic and magic magmatism and high-pressure metamorphism associated with this Caledonian orogenic cycle (480-450 Ma) are identified in the Alpine basement units, the exact geodynamic setting remains unclear (Schaltegger et al., 2003). While the debate about subduction polarity persist, it is clear whether crustal fragments were accreted to the Gondwanan margin during the Caledonian orogeny (Schaltegger et al., 2003).

2.2.3 Variscan Orogeny

While the Cadomian and Caledonian orogenies left limited imprints on the Alpine basement, the Variscan orogeny impacted large portions of pre-Alpine crustal basement units in a major way (von Raumer, 1998; von Raumer et al., 2002). The Variscan orogen was the result

https://doi.org/10.5194/se-2020-44
Preprint. Discussion started: 29 April 2020

of the collision between the Gondwana and Laurussia/Avalonia continental plates, which resulted in the formation of the super-continent Pangea (Franke, 2006). The closure of the Paleo-tethys and the Rheno-hercynian oceans, leading to the formation of Pangea, started at ~400 Ma and ended in a continent-continent collision at 300 Ma. It was characterized by voluminous syn- and post-orogenic plutonic magmatism (Franke, 2006;von Raumer et al., 2009 and references therein). The final stage of post-orogenic Variscan magmatism lasted until ~250 Ma (Finger et al., 1997). The Aar and Gotthard external massifs, located south of the central Swiss study location (Figure 1), contain voluminous Variscan U-Pb plutonic rocks (Schaltegger, 1994). While the external massifs of the northern part of Central Alps also contain abundant Variscan crustal material (von Raumer et al., 2003; Engi et al., 2004; Franke, 2006), they were not exposed to erosion until ~14 Ma (Stutenbecker et al., 2019).

2.2.4 Alpine Orogeny

The collision history between the European and Adriatic continental plates commenced in the Late Cretaceous with the closure of portions of the Alpine Tethys and subduction of the European plate beneath the Adriatic continental plate (Schmid et al., 1996). This Eo-Alpine subduction resulted in blueschist and eclogite facies metamorphism (Ring, 1992; Engi et al., 1995; Rubatto et al., 2011) preserved in slivers between the Penninic nappe stack of the Lepontine (e.g., Cima-Lunga nappe; Schmid et al., 1996). The main Alpine continent-continent collision started at ~33 Ma, when the European continental lithosphere started to enter the subduction channel (Schmid et al., 1996). The buoyancy differences between the oceanic lithosphere and the buoyant continental lithosphere potentially resulted in oceanic slab break-off and at a resulting magmatic flare-up at ~32 Ma (Davis and Blanckenburg, 1995; Schmid et al., 1996). The subsequent advection of heat resulted in a Barrovian-type high-grade metamorphism in the area of the Lepontine dome (Frey et al., 1980; Hurford, 1986; Kissling and Schlunegger, 2018).

The Helvetic thrust nappes, overthrust by Penninc and Austroalpine nappes prior to the time of slab breakoff, experienced greenschist and prehnite-pumpellyite metamorphism between 35 and 30 Ma (Frey et al., 1980; Groshong and Brawn, 1984; Hunziker et al., 1992). Emplacement and thrusting of the Helvetic nappes along the basal Alpine thrust on the proximal

https://doi.org/10.5194/se-2020-44
Preprint. Discussion started: 29 April 2020

European margin (Figure 1) occurred between 25 and 20 Ma and resulted in a greenschist overprint of the basement in the external massifs (Niggli and Niggli, 1965; Frey et al., 1980; Rahn et al., 1994). A late-stage phase of basement-involved duplexing resulted in the rise of the external massifs and the final shape of the Central Alps (Herwegh et al., 2017; Mair et al., 2018; Herwegh et al., 2019).

3 Molasse Basin: Architecture, Stratigraphy, and Provenance

The Molasse basin extends ~600 km from Lake Geneva to the Bohemian massif (Kuhleman and Kempf, 2002; Figure 1). The Swiss part of the Molasse Basin, a sub-section of this foreland trough, is located between Lake Geneva and Lake Constance and is the focus of this study. It is flanked in the north by the Jura Mountains and in the south by the Central Alps. The basin is commonly divided into the Plateau Molasse, the undeformed central basin, and the Subalpine Molasse, the deformed basin adjacent to the Central Alps. The Cenozoic strata of the flexural Swiss Molasse basin have been divided into five lithostratigraphic units that are (oldest to youngest): the North Helvetic Flysch (NHF), the Lower Marine Molasse (LMM), the Lower Freshwater Molasse (LFM), the Upper Marine Molasse (UMM), and the Upper Freshwater Molasse (UFM) (Figure 2; Sinclair and Allen, 1992). Overall, they record two large-scale shallowing- and coarsening-upward sequences that formed in response to Alpine tectonic processes and changes in sediment supply rates (Matter et al., 1980; Pfiffner, 1986; Sinclair and Allen, 1992; Sinclair et al., 1997; Kuhlemann and Kempf, 2002; Garefalakis and Schlunegger, 2018).

3.1 North Helvetic Flysch

The earliest foreland basin deposits comprise the North Helvetic Flysch (NHF) with initial turbidite deposition starting in the Middle to Late Eocene (Allen et al., 1991). During that time, clastic deep-water sediments accumulated along the attenuated European continental margin (Crampton and Allen, 1995). The NHF was sourced from the approaching earliest Alpine thrust sheets (Allen et al., 1991). In central Switzerland, the NHF includes sandstone, shale, and some volcanic detritus derived from the volcanic arc situated on the Adriatic plate at that time (Lu et al., 2018; Reichenwallner, 2019). The initial deep-marine, turbiditic clastic deposits exhibit orogen-parallel transport from the west (Sinclair and Allen, 1992). Currently, NHF strata

https://doi.org/10.5194/se-2020-44
Preprint. Discussion started: 29 April 2020

in the region are highly deformed and tectonically located below the Helvetic thrust nappes (Pfiffner, 1986).

3.2 Lower Marine Molasse

After deep-marine deposition of the NHF, sedimentation associated with the Lower Marine Molasse (LMM) continued in an underfilled flexural foredeep (Sinclair et al., 1997). From 34-30 Ma (Pfiffner et al., 2002 and references therein) deposition of the LMM progressively transitioned from deep-marine turbidites to tabular and cross-bedded sandstones with symmetrical wave ripples (Matter et al., 1980; Diem, 1986) recording a storm- and wave-dominated shallow-marine environment (Diem, 1986; Schlunegger et al., 2007). The LMM strata record paleocurrent directions that were mostly perpendicular to the orogenic front with a NE-directed tendency (Trümpy et al., 1980; Diem, 1986; Kempf et al., 1999). Sandstone provenance of the LMM suggests mainly derivation from recycled Penninic sedimentary rocks situated along the Alpine front at the time (Matter et al. 1980; Gasser, 1968). Outcrops of the LMM are restricted to the deformed wedge of the Subalpine Molasse.

Increased sediment supply in response to rapid erosion of the emerging Alpine orogenic wedge resulted in overfilling of the Swiss Molasse basin, signaling the shift from the LMM to the fluvial and alluvial deposits of the Lower Freshwater Molasse (LFM) (Sinclair and Allen, 1992; Sinclair et al., 1997; Kuhlemann and Kempf, 2002; Schlunegger and Castelltort, 2016; Garefalakis and Schlunegger, 2018). The transition to the LFM was also characterized by the first-appearance of Alpine derived conglomerates at ~30 Ma in central Switzerland (Schlunegger et al., 1997a; Kempf et al., 1999; Kuhlemann and Kempf, 2002).

3.3 Lower Freshwater Molasse

Within the Swiss Molasse basin, the deposition of the Lower Freshwater Molasse (LFM) occurred between ~30 to 20 Ma (Kempf et al., 1999). A regional hiatus separated these older pre-25 Ma (LFM I) from the younger post-24 Ma fluvial deposits (LFM II) (Schlunegger et al., 1997a). In central Switzerland an ~4 km wedge of the LFM is preserved (Stürm, 1973), with the thickest exposed LFM suites occurring in the Subalpine Molasse belt adjacent to the thrust front, such as the Rigi and Höhronen conglomeratic megafans (and others) (Schlunegger et al., 1997b, c). During the ~25-24 Ma hiatus, deposition switched from the Rigi to the Höhronen fan

https://doi.org/10.5194/se-2020-44
Preprint. Discussion started: 29 April 2020

(Schlunegger et al., 1997b, c). Alluvial fan deposition transitioned to channel conglomerates and sandstones away from the thrust front (Büchi and Schlanke, 1977; Platt and Keller, 1992). Limestone, metamorphic, igneous, and ophiolitic clasts derived from the Penninic and Austroalpine units dominated LFM alluvial fan conglomerates (e.g., von Eynatten et al., 1999; Spiegel et al., 2004). Flysch sandstone clasts recycled in the LFM also indicate erosion of older Penninc flysch units (Gasser, 1968). A marked change in clast LFM composition occurred at ~24 Ma, with the switch from >80% sedimentary clasts in the Rigi fan prior to 25 Ma (Stürm, 1973) to >50-60% crystalline granitic clasts in the Höhronen fan thereafter (Schlunegger et al., 1997a; Von Eynatten and Wijbrans, 2003). After ~22 Ma, rapid, large-magnitude tectonic exhumation of the Lepontine Dome, in response to syn-orogenic extensions (Mancktelow and Grasemann, 1997), led to widespread exposure of the Penninic core complex as evidenced by Alpine-aged detrital mica $^{40}Ar/^{39}Ar$ ages in the Molasse basin (Von Eynatten et al., 1999). At ~21 Ma (LFM IIb), a significant shift in provenance was signaled by a transition in sandstone heavy mineral compositions, as epidote started to dominate the heavy mineral suite by more than 90 percent (Fuchtbauer, 1964; Schlanke, 1974; Kempf et al., 1999). This shift was also accompanied by a trend toward more fine-grained sedimentation (Schlunegger et al., 1997a). However, implications of this shift in provenance have been non-conclusive, as Renz (1937), Füchtbauer (1964), and Dietrich (1969) suggested that the epidote minerals were derived from Penninic ophiolites, while Füchtbauer (1964) claimed sourcing from crystalline and greenschist units in the Austroalpine nappes.

3.4 Upper Marine Molasse

Continental deposition of the LFM was followed by a shift to marine sedimentation of the Upper Marine Molasse (UMM) in the Swiss foreland basin (Keller, 1989). This has been interpreted as a change back to underfilled conditions. A return towards an underfilled basin started already during LFM times at ~21 and was characterized by a continuous reduction in sediment supply rates (Kuhlemann, 2000;Willett and Schlunegger, 2010). Marine conditions began in the eastern Molasse basin and propagated westward (Strunck and Matter, 2002; Garefalakis and Schlunegger, 2019). These related effects appear to have been amplified by a tectonically-controlled widening of the basin (Garefalakis and Schlunegger, 2019). This change from overfilled non-marine to under-filled marine conditions is referred to as the Burdigalian

https://doi.org/10.5194/se-2020-44
Preprint. Discussion started: 29 April 2020

Transgression (Sinclair et al., 1991). However, the debate continues whether the cause of the Burdigalian Transgression is due to: (i) an increase in sea level outpacing sedimentation (Jin et al., 1995; Zweigel et al., 1998), (ii) an increase in tectonic loading through thrusting of the external massifs (Sinclair et al., 1991), or (iii) an increase in slab pull causing more flexure of the European plate paired with a reduction in sediment supply and a rising eustatic sea level (Garefalakis and Schlunegger, 2019).

The Burdigalian Transgression resulted in the deposition of wave and tide-dominated sandstones in a shallow marine environment (Allen et al., 1985; Homewood et al., 1986; Keller, 1989; Jost et al., 2016; Garefalakis and Schlunegger, 2019). At the thrust front these shallow-marine sandstones interfinger with fan delta deposits. Shallow-marine deposition lasted until ~17 Ma (Schlunegger et al., 1997c). Heavy mineral data (Allen et al., 1985) and clast petrography analysis (Matter, 1964), in conjunction with measurements of clast orientations in conglomerates and cross-beds in sandstones (Allen et al., 1985; Garefalakis and Schlunegger, 2019), reveal that the UMM of Switzerland was a semi-closed basin. Detritus sourced from the Central Alps was deposited adjacent to the fan deltas and reworked by waves and tidal currents.

3.5 Upper Freshwater Molasse

The Upper Freshwater Molasse (UFM) consists of non-marine conglomerates and sandstones deposited in prograding alluvial fans and fluvial floodplains (Keller, 2000). The thickest section of the preserved UFM (~1500 m) is situated to the west of Lucerne (Matter, 1964; Trümpy, 1980). Geochemistry of detrital garnet in the UFM record the first signal of erosion of the external massifs by ~14 Ma at the latest (Stutenbecker et al., 2019).

Deposition of the UFM in central Switzerland is only recorded until ~12 Ma (Schlunegger et al., 1996) as younger strata were eroded from the region (e.g. Burkhard and Sommaruga, 1998; Cederbom et al., 2004; Cederbom et al., 2011). Vitrinite reflectance and apatite fission track borehole data from the Molasse basin suggest that up to 700 m of UFM strata were removed by erosion (Schegg et al., 1999; Cederbom et al., 2004; 2011). Erosion of the basin fill started in the Late Miocene to Pliocene (Mazurek et al., 2006; Cederbom et al., 2011) after active thrusting propagated to the Jura Mountains, and the Molasse basin essentially became a piggy-back basin (Burkhard and Sommaruga, 1998; Pfiffner et al., 2002), or alternatively a negative alpha basin (Willett and Schlunegger, 2011).

https://doi.org/10.5194/se-2020-44
Preprint. Discussion started: 29 April 2020

4 Sampling Strategy and Methodology

4.1 Sampling Strategy

Samples were collected along the southern portion of the basin within the Plateau Molasse, the Subalpine Molasse, and the North Helvetic Flysch. Three sections were sampled: The Lucerne Section in central Switzerland, the Thun Section in west-central Switzerland, and the Bregenz Section in westernmost Austria (Figures 1 and 3; Table 1). Sampling in the Lucerne Section was accomplished to cover the full range in depositional ages from the North Helvetic Flysch to the Upper Freshwater Molasse, spanning between 34 and 13.5 Ma with less than a 2-5 myr time resolution. Sample sites in the Bregenz Section covered the major lithostratigraphic groups of the Molasse deposits at a lower resolution, while samples from the Thun Section comprised only the LFM and terrestrial equivalents of the UMM deposits for along-strike comparison purposes. All separated samples contained detrital zircon and were used for U-Pb age dating. Stratigraphic age assignments for the samples for the Lucerne Section were based on the chronological framework from Schlunegger et al. (1997a), established in the Lucerne area through detailed magneto- and biostratigraphy (e.g., Weggis, Rigi, and Höhrone conglomerates; LFM I and LFM IIa/IIb units). Ages were projected into the Lucerne Section through mapping and balanced cross section restorations. Chronostratigraphic age constraints for the UMM sandstones were taken from Keller (1989), Jost et al. (2016) and Garefalakis and Schlunegger (2019). Precise ages for the UFM units are not available and they could comprise the entire range between 17 Ma (base of UFM) and ~13 Ma (youngest LFM deposits in Switzerland; Kempf and Matter (1999)). The chronological framework for the Molasse units for the Thun section is based on litho- and chronostratigraphic work by Schlunegger et al. (1993, 1996). There, OA13-samples were collected along the magnetostratigraphic section of Schlunegger et al. (1996) with an age precision of ~0.5 Ma. Sample site 10SMB07 was collected from a conglomerate unit, mapped (Beck and Rutsch, 1949) as a terrestrial equivalent of the UMM (Burdigalian), although the depositional age could also correspond to the UFM (Langhian), as indicated by litho- and seismostratigraphic and heavy mineral data from a deep well (Schlunegger et al., 1993). Site 10SMB06 comprises a suite of conglomerates with quartzite clasts - their first appearance was dated to ~25 Ma in the adjacent thrust sheet to the South (Schlunegger et al., 1996). While, deposition of quartzite clasts, however, continues well into the UFM (Matter, 1964), the quartzite

https://doi.org/10.5194/se-2020-44
Preprint. Discussion started: 29 April 2020

Solid Earth Discussions
Open Access
EGU

conglomerates in the Thun section (10SMB06) directly overly sandstones of the LMF II as a tectonic interpretation of a seismic section has revealed (Schlunegger et al., 1993). Therefore, we tentatively assigned an LMF II age to the 10SMB06 sample site. Finally, sampling and stratigraphic age assignments for samples from the Bregenz Section were guided by the geological map of Oberhauser (1994) and by additional chronologic (Kempf et al., 1999) and stratigraphic work (Schaad et al., 1992). We considered an uncertainty of ±2 Ma to the age assignment for the Bregenz Section samples.

4.2 Zircon U-Pb LA-ICPMS Methodology

The bulk of the detrital zircon samples were analyzed at the UTChron geochronology facility in the Department of Geological Sciences at the University of Texas at Austin and a smaller subset at the at the Isotope Geochemistry Lab (IGL) in the Department of Geology at the University of Kansas, using identical instrumentation and very similar analytical procedures, but different data reduction software (Table 1). All samples underwent conventional heavy mineral separation, including crushing, grinding, water-tabling, magnetic, and heavy liquid separations, but no sieving at any point. Separate zircon grains were mounted on double-sided tape (tape-mount) on a 1" acrylic or epoxy disc without polishing. For all samples 120-140 grains were randomly selected for LA-ICPMS analysis to avoid biases and capturing all major age components (>5%) (Vermeesch, 2004). All grains were depth-profiled using a Photon Machines Analyte G2 ATLex 300si ArF 193 nm Excimer Laser combined with a ThermoElement 2 single collector, magnetic sector -ICP-MS, following analytical protocols of Marsh and Stockli (2015). 30 seconds of background was measured followed by 10 pre-ablation "cleaning" shots, then 15 sec of washout to measure background, prior to 30 sec of sample analysis. Each grain was ablated for 30 seconds using a 30 µm spot with a fluence of ~4 J/cm2, resulting in ~20 µm deep ablation pits. For U-Pb geochronologic analyses of detrital zircon the masses ^{202}Hg, ^{204}Pb, ^{206}Pb, ^{207}Pb, ^{208}Pb, ^{232}Th, ^{235}U, and ^{238}U were measured.

GJ1 was used as primary zircon standard (^{206}Pb/^{238}U 601.7 ± 1.3 Ma, ^{207}Pb/^{206}Pb 607 ± 4 Ma; Jackson et al. 2004) and interspersed every 3-4 unknown analyses for elemental and depth-dependent fractionation. Plesovice (337.1 ± 0.4 Ma, Slama et al., 2008) was used as a secondary standard for quality control, yielding ^{206}Pb/^{238}U ages during this study of 338 ± 6 Ma, which is in agreement with the published age. No common Pb correction was applied. At UTChron, data

https://doi.org/10.5194/se-2020-44
Preprint. Discussion started: 29 April 2020

reduction was performed using the IgorPro (Paton et al., 2010) based Iolite 3.4 software with Visual Age data reduction scheme (Petrus & Kamber, 2012), while at KU's IGL U-Pb data were reduced using Pepiage (Dunkl et al., 2009) or Iolite employing an Andersen (2002) correction method and decay constants from (Steiger and Jäger, 1977). The Andersen (2002) correction method iteratively calculates the $^{208}Pb/^{232}Th$, $^{207}Pb/^{235}U$, and $^{206}Pb/^{238}U$ ages to correct for common-Pb where ^{204}Pb cannot be accurately measured. Sample 09SFB11 was reduced using Pepiage and for this reason U ppm and U/Th ratio were not calculated.

All uncertainties are quoted at 2σ and age uncertainty of reference materials are not propagated. For ages younger than 850 Ma, $^{206}Pb/^{238}U$ ages are reported and grains were eliminated from text and figures if there was greater than 10% discordance between the $^{206}Pb/^{238}U$ age and the $^{207}Pb/^{235}U$ age or the $^{206}Pb/^{238}U$ age had greater than 10% 2σ absolute error. For ages older than 850 Ma, $^{207}Pb/^{206}Pb$ ages are reported and grains were eliminated from text and figures if there was greater than 20% discordance between $^{206}Pb/^{238}U$ age and $^{207}Pb/^{206}Pb$ age. Analytical data were visually inspected for common Pb, inheritance, or Pb loss using the VizualAge live concordia function (Petrus and Kamber, 2012). Laser Ablation-ICPMS depth profiling allows for the definition of more than one age from a single grain, hence ages in Supplemental File 1 are labelled either single age, rim, or core. Commonly a single concordant age was obtained for each zircon; however, if more than one concordant age was defined then both analyses were included in the data reporting.

4.3 Laser Ablation-Split Stream (LASS) Analyses of Detrital Zircon

In an attempt to glean additional provenance constraints from Molasse samples, we also combined U-Pb with Trace Element (TE) and Rare Earth Element (REE) analyses on the same grain for select samples via laser ablation split-steam (LASS) U-Pb analysis at the University of Texas at Austin (Marsh and Stockli, 2015). Combined U-Pb isotopic and TE/REE data can help improve provenance resolution on the basis of petrogenic affiliations of individual grains (Kylander-Clark et al., 2013). For LASS analysis, ablated aerosols were divided between two identical ThermoFisher Element2 single collector, magnetic sector-ICP-MS instruments and analyzed for ^{29}Si, ^{49}Ti, ^{89}Y, ^{137}Ba, ^{139}La, ^{140}Ce, ^{141}Pr, ^{146}Nd, ^{147}Sm, ^{153}Eu, ^{157}Gd, ^{159}Tb, ^{163}Dy, ^{165}Ho, ^{166}Er, ^{169}Tm, ^{172}Yb, ^{175}Lu, ^{178}Hf, ^{181}Ta, ^{232}Th, and ^{238}U. Data generated from the TE and REE analyses were reduced using the "Trace_Elements_IS" data reduction scheme from Iolite

https://doi.org/10.5194/se-2020-44
Preprint. Discussion started: 29 April 2020

(Paton et al., 2011), using ^{29}Si as an internal standard indexed at 15.3216 wt.% ^{29}Si. NIST612 was used as the primary reference material and GJ1 and Pak1 as secondary standards to verify data accuracy.

4.4 Zircon Elemental Analysis

While studies (e.g. Hoskin and Ireland, 2000; Belousova et al., 2002) have shown that zircon REE patterns in general do not show systematic diagnostic variations as a function of different continental crustal rock types (von Eynatten and Dunkl, 2012), it has been shown that TE and REE can be used to differentiate between igneous zircon from continental (e.g., arc), oceanic, and island arc tectono-magmatic environments (Grimes et al., 2015). Furthermore, trace elements and REEs can be used to fingerprint zircon with mantle affinity (i.e., kimberlites and carbonatites; Hoskin and Ireland, 2000), hydrothermal zircon (Hoskin, 2005), or zircon that grew or recrystallized under high-grade metamorphic conditions (Rubatto, 2002). Furthermore, Ce and Eu anomalies in zircons have been used as proxies for magmatic oxidation states (Trail et al., 2012; Zhong et al., 2019) and Ti-in-zircon as a crystallization thermometer (Watson et al., 2006). Detrital studies have utilized these techniques to identify characteristic zircon signatures from non-typical sources (e.g. Anfinson et al., 2016; Barber et al., 2019).

Chondrite-normalized REE zircon signatures were only considered for concordant U-Pb ages as metamictization likely also affected REE and TE spectra. Zircon with anomalously elevated and flat LREE (La-Gd) concentrations were excluded from figures and interpretations as these are likely due to mineral inclusions (i.e. apatite) or hydrothermal alteration (Bell et al., 2019).

5 Detrital U-Pb Age Groups and Associated Orogenic Cycles

In an attempt to simplify data presentation and data reporting, the detrital zircon U-Pb ages were lumped into genetically-related tectono-magmatic age groups that include the Variscan, Caledonian, and Cadomian orogenic cycles. In addition to these three pre-Alpine orogenic cycles we also considered the total number of Cenozoic (Alpine) ages, Mesozoic (Tethyan) ages, and pre-Cadomian ages. The following sections provide a brief description of the different delineated age groups. While there can be considerable debate regarding the exact duration of orogenic cycles (Dewey and Horsfield, 1970), grouping zircon U-Pb according to

https://doi.org/10.5194/se-2020-44
Preprint. Discussion started: 29 April 2020

their tectono-magmatic or orogenic affinity provides a convenient way to discuss potential detrital sources. The informal age ranges adopted in this study are Cenozoic (0 to 66 Ma), Mesozoic (66 to 252 Ma), late Variscan (252 to 300 Ma), early Variscan (300-370 Ma) Caledonian (370 to 490 Ma), Cadomian (490 to 710 Ma), and Pre-Cadomian (>710 Ma). We simplified these age groups to represent a continuous series with no time gaps and to ensure no omission of ages and for simplicity of depicting ages using the DetritalPy software of Sharman et al. (2018b). Abundant Variscan zircon U-Pb ages are split into two groups (late Variscan and early Variscan) to reflect differences between syn- and post-orogenic magmatism on the basis of discussion of Finger et al. (1997). Finger et al. (1997) noted five generalized genetic groups of granitoid production during the Variscan Orogeny: 1) Late-Devonian to Early Carboniferous I-type granitoids (370 to 340 Ma), 2) Early Carboniferous deformed S-type granitoids (~340 Ma), 3) Late Visian-Early Namurian S-type and high-K I-type granitoids (340 Ma to 310 Ma), 4) Post-collisional I-type granitoids and tonalites (310-290 Ma), and 5) Late Carboniferous to Permian leucogranites (300-250 Ma). The general age ranges of the Caledonian (370 to 490 Ma) and Cadomian (490 to 710 Ma) orogens are based on Pfiffner (2014), McCann (2008), Krawczyk et al. (2008), and Stephan et al. (2019). While uncertainties and discordance of LA-ICPMS U-Pb ages allow for overlap between these groupings, they provide a potential and viable way to depict and estimate detrital zircon contributions from these different source regions and to identify potential provenance changes in the Molasse basin.

6 Detrital Zircon U-Pb Ages

6.1 Lucerne Section (Central Switzerland; Sample Locations: Figure 3a; U-Pb Data: Figure 4)

For data presentation, we grouped the detrital zircon U-Pb ages according to their lithostratigraphic units for simplicity as there is little variation in DZ U-Pb age signatures within individual units. The detrital zircon U-Pb ages of individual samples can be found in Supplemental File 1 and all associated sample information can be found in Table 1.

6.1.1 Northern Helvetic Flysch (NHF)

Samples 09SFB43 and 09SFB02 were collected from the Northern Helvetic Flysch and have a depositional age of 35 ± 3 Ma. The samples contain a total of 261 concordant U-Pb ages

https://doi.org/10.5194/se-2020-44
Preprint. Discussion started: 29 April 2020

ranging from 34.8 to 2838 Ma and can be binned in the flowing tectono-magmatic groups discussed in the Section 4: Cenozoic (4.2%), Mesozoic (0.8%), Late Variscan (9.6%), Early Variscan (5%), Caledonian (29.1%), Cadomian (37.9%), and pre-Cadomian (13.4%). Notably, there are eleven grains with ages between 34.8 and 37.3 Ma in sample 09SFB43 that fall within uncertainty of the depositional age.

6.1.2 Lower Marine Molasse

Sample 09SFB10b was collected from the Lower Marine Molasse and has a depositional age of 32 ± 1 Ma. The sample contains a total of 114 concordant U-Pb zircon ages ranging from 243.6 to 2611 Ma. There were no Cenozoic grains, two Mesozoic ages at 243.6 and 243.7 Ma and two Permian ages at 287.2 and 294.6. The age spectrum is composed of the following age groups with the following percentages: Mesozoic (1.8%), Late Variscan (1.8%), Early Variscan (17.5%), Caledonian (36%), Cadomian (23.7%), and pre-Cadomian (19.3%).

6.1.3 Lower Freshwater Molasse

Samples 09SFB45 and 09SFB21 were collected from the lower units of the Lower Freshwater Molasse and have depositional ages of 27 ± 1 Ma (LFM I) and 22.5 ± 1 Ma (LFM IIa), respectively. The combined samples contain a total of 202 concordant ages ranging from 191.7 to 2821 Ma. The sample yielded no Cenozoic grains and four Mesozoic grains with ages ranging from 191.7 to 243.1 Ma. The rest of the grains fall into the following age groups Mesozoic (2%), Late Variscan (9.4%), Early Variscan (13.9%), Caledonian (25.7%), Cadomian (26.2%), and Pre-Cadomian (19.3%).

Samples 09SFB13, 09SFB08 and 09SFB33 were collected from Unit IIb of the Lower Freshwater Molasse and have depositional ages of 21.5 ± 1 Ma, 21.5 ± 1 Ma and 21 ± 1 Ma, respectively. The combined samples contain a total of 505 concordant U-Pb analyses ranging in age from 222.7 to 2700 Ma. There were not Cenozoic ages and eleven Triassic ages ranging from 222.7 Ma to 251.6 Ma - 9 of these 11 grains had >900 ppm U and were considered suspect for possible Pb loss. The age spectrum is composed of the following age groups and proportions: Mesozoic (2%), Late Variscan (53.3%), Early Variscan (10.5%), Caledonian (15.0%), Cadomian (11.7%), and Pre-Cadomian (7.3%).

https://doi.org/10.5194/se-2020-44
Preprint. Discussion started: 29 April 2020

6.1.5 Upper Marine Molasse

Samples 09SFB05, 09SFB29, 09SFB49, and 09SFB14 were collected from the Upper Marine Molasse and have depositional ages of 20 ± 1 Ma, 19 ± 1 Ma, 19 ± 1 Ma, and 17.5 ± 1 Ma, respectively. These combined samples contain a total of 356 concordant ages ranging in age from 162.1 Ma to 2470 Ma. There are no Cenozoic grains, two Jurassic ages (162.1 Ma and 165.9 Ma) and seventeen Triassic ages that range from 210.7 Ma to 251.6 Ma. Overall, theses ages fall into the following groups: Mesozoic (5.3%), Late Variscan (41.1%), Early Variscan (14.3%), Caledonian (13.8%), Cadomian (15.7%), and Pre-Cadomian (6.7%).

6.1.6 Upper Freshwater Molasse

Samples 09SFB12, 09SFB07, 09SFB11, and 09SFB38 were all collected from the Upper Freshwater Molasse and have depositional ages of 16 ± 1 Ma, 15.5 ± 1 Ma, 14 ± 1 Ma, and 13.5 ± 1 Ma, respectively. These combined samples contain a total of 364 concordant ages ranging from 30.6 Ma to 3059.9 Ma and yielded a single Cenozoic age (30.6 Ma), a single Cretaceous age (130.7 Ma), a single Jurassic age (148.3 Ma), and fourteen Triassic ages that range from 207.8.7 Ma to 251.7 Ma. Overall, the age groups are characterized by the following proportions: Cenozoic (0.3%), Mesozoic (4.4%), Late Variscan (36%), Early Variscan (20%), Caledonian (18.4%), Cadomian (14%), and Pre-Cadomian (6.9%).

6.2 Thun Section (West-Central Switzerland; Sample Locations: Figure 3b; U-Pb Data: Figure 5)

6.2.1 Lower Freshwater Molasse

Samples 13SFB03, 13SFB04, and 10SMB06 were collected from the Lower Freshwater Molasse and have depositional ages of 28 ± 0.5 Ma, 26 ± 0.5 Ma and 22 ± 2.5 Ma, respectively. The combined samples contain a total of 344 concordant ages ranging from 217.8 to 3304 Ma, falling into the following age groups: Mesozoic (2%), Late Variscan (18%), Early Variscan (23%), Caledonian (26.2%), Cadomian (20.9%), and Pre-Cadomian (9.9%).

6.2.2 Terrestrial Equivalents of the Upper Marine Molasse and Upper Freshwater Molasse

Sample 10SMB07 was collected from the terrestrial equivalent of the Upper Marine Molasse and Upper Freshwater Molasse and has a depositional age of 18 ± 3 Ma. A large

https://doi.org/10.5194/se-2020-44
Preprint. Discussion started: 29 April 2020

number of grains were discordant and hence the sample yielded only a total of 53 concordant ages ranging from 186.1 to 2688.2 Ma. The age groups represented were Mesozoic (3.8%), Late Variscan (49.1%), Early Variscan (22.6%), Caledonian (9.4%), Cadomian (7.5%), and Pre-Cadomian (7.5%).

6.3 Bregenz Section (Western Austria; Sample Locations: Figure 3c; U-Pb Data: Figure 6)

6.3.1 Lower Marine Molasse

Sample 10SMB12 was collected from the Lower Marine Molasse and has a depositional age of 32 ± 2 Ma. The sample contains a total of 98 concordant ages ranging from 36.3 to 2702 Ma. It was characterized by the age groups and percentages: Cenozoic (1%), Mesozoic (1%), Late Variscan (7.1%), Early Variscan (13.3%), Caledonian (17.3%), Cadomian (25.5%), and Pre-Cadomian (34.7%). Remarkable was an anomalously large percentage of Mesoproterozoic (11.2%) and Paleoproterozoic (12.2%) ages.

6.3.2 Lower Freshwater Molasse

Sample 10SMB11 was collected from the Lower Freshwater Molasse and has a depositional age of 22 ± 2 Ma. The sample contains a total of 70 concordant ages ranging from 217.5 to 2172 Ma, falling into the following groups with the following percentages: Mesozoic (1.4%), Late Variscan (12.9%), Early Variscan (27.1%), Caledonian (27.1%), Cadomian (14.3%), and Pre-Cadomian (17.1%).

5.3.3 Upper Marine Molasse

Sample 10SMB10 was collected from the Upper Marine Molasse and has a depositional age of 19 ± 2 Ma. The sample contains a total of 161 concordant ages ranging from 234.3 to 2837 Ma. It is characterized by the following age group and percentages: Mesozoic (0.8%), Late Variscan (13.7%), Early Variscan (21.1%), Caledonian (24.2%), Cadomian (19.9%), and Pre-Cadomian (20.5%).

6.3.3 Upper Freshwater Molasse

Sample 10SMB09 was collected from the Upper Freshwater Molasse and has a depositional age of 15 ± 2 Ma. The sample contains a total of 81 concordant ages ranging from

https://doi.org/10.5194/se-2020-44
Preprint. Discussion started: 29 April 2020

257.7.3 to 2030 Ma, characterized by the following age groups and percentages: Late Variscan (12.3%), Early Variscan (48.1%), Caledonian (11.1%), Cadomian (16%), and Pre-Cadomian (12.3%). Notably, the sample lacked any Cenozoic or Mesozoic zircons.

7 Detrital Zircon Geochemistry and Rim-Core relationships

Individual zircon grains often record multiple growth episodes in response to magmatic or metamorphic events within a single source terrane. Recovery of these multi-event source signatures from a single zircon allow for improved pinpointing of detrital provenance and a more completing understanding of the source terrane history. Laser-Ablation Split-Stream (LASS) Depth Profiling by ICP-MS has enabled for a more systematic harvesting of these relationships and hence complete picture of the growth of the detrital zircon grains (e.g. Anfinson et al. 2016; Barber et al. 2019). We applied this to methodology to samples of the Lucerne Section following the analytical procedures of Marsh and Stockli (2015) and Soto-Kerans et al. (2020). For discussion purposes, these data were divided into two groups: (1) depositional ages >22 Ma and (2) depositional ages <22 Ma. For depositional ages >22 Ma, the geochemical data were drawn from the REE analyses of four samples (approximate depositional age in parentheses): 09SFB33 (21 Ma), 09SFB49 (19 Ma). 09SFB14 (17.5 Ma), and 09SFB38 (13.5 Ma). For depositional ages >22 Ma, the geochemical data were drawn from samples 09SFB45 (27 Ma) and 09SFB21 (22.5 Ma). Detrital zircon grains that have experienced hydrothermal alteration or contamination of the zircon profile by exotic mineral inclusion (e.g. apatite) commonly show high, flat light rare earth element (LREE) patterns (Hoskin and Ireland, 2000; Bell et al., 2019). We have removed these altered profiles from the data plots but show all data in Supplemental File 2.

7.1 Depositional Ages >22 Ma

The REE data show that Variscan detrital zircons are mainly magmatic in origin as indicted by comparison to REE profiles from Belousova et al. (2002) and Hoskin and Ireland (2000). There is little to no evidence for metamorphic/metasomatic zircon grains (Figure 7a). In contrast, Cadomian and in particular Caledonian zircon grains exhibit elevated U-Th values (Figure 8b). Only a single Caledonian grain with a 468 Ma U-Pb age (sample SFB21) is characterized by a depleted HREE profile (Fig 7c) indicative of metamorphic growth in the presence of garnet (e.g. Rubatto, 2002). There is little evidence of mafic zircon sources, as the U

https://doi.org/10.5194/se-2020-44
Preprint. Discussion started: 29 April 2020

ppm and TE values and typically more characteristic of arc magmatism (e.g. Grimes et al. 2015; Barber et al., 2019). For depositional ages older than 22 Ma there is a minor number of Variscan rims on Cadomian and Caledonian cores (Figure 9).

7.2 Depositional Ages <22 Ma

Similar to the pre-Miocene detrital zircon, LASS-ICP-MS geochemical data from the younger stratigraphic samples (<22 Ma) suggest that Variscan detrital zircons are primarily of magmatic origin. However, compared to the older samples, there is evidence for increasing input of metamorphic/metasomatic grains (Figure 7b). Sample 09SFB14 contained one Variscan grain (262 Ma U-Pb age) and the youngest Molasse sample (09SFB38; ca. 13.5 Ma) three Variscan zircons (316-329 Ma) with depleted HREE profiles. 09SFB38 also has a higher percentage of Variscan grains with elevated U/Th values (Figure 8a). Together, these data indicate a slight increase in the input of metamorphic Variscan sources through time. However, there is no evidence for the input of neither magmatic nor metamorphic Alpine zircons or zircon rims.

The geochemical data of Caledonian and Cadomian detrital zircons from these Miocene samples also are consistent with primarily a magmatic origin with a subordinate number of detrital zircon grains exhibiting elevated U/Th values (Figure 8b). However, there is little evidence for metamorphic grains from the REE profiles (Figure 7d).

Overall, the vast majority of all detrital zircon grains are interpreted to have a typical magmatic REE profile, with positive Ce and negative Eu anomalies, and overall positive slopes, including positive MREE-HREE slopes. The U/Th from all detrital zircon grains are consistent with predominately magmatic characters. In summary, the REE data suggest that detrital zircons from all three recent orogenic cycles are primarily magmatic in origin with very limited metamorphic zircon input. For depositional ages younger than 22 Ma there is a noticeable increase in Variscan rims on Caledonian, Cadomian, and Proterozoic cores (Figure 9).

8 Discussion

Progressive changes in detrital zircon U-Pb age patterns in the Molasse Basin allow for new insights and a refinement of the reconstruction of the evolution of drainage networks of the Central Alps during the Alpine orogenesis. Central to this discussion is the salient observation that within the Lucerne Section a remarkable shift is observed in the detrital zircon U-Pb age signatures at ~ 22 Ma. Prior to that time, detrital zircon ages included the entire range of pre-Cadomian, Cadomian, Caledonian, Variscan ages in similar proportions (Figure 4). In addition, there was little variation in zircon age patterns from sample to sample in the Molasse strata deposited prior to 22 Ma. Noteworthy is the occurrence of ~34 Ma-old North Helvetic Flysch sample 09SFB43, that are essentially contemporaneous with the depositional age and make up ~8% of the detrital zircon grains (Figure 4). In contrast, after 22 Ma, detrital zircon ages are dominated by late Variscan ages and limited contributions of older detrital zircon grains. The trend of increasing late Variscan ages is nicely depicted in the Multidimensional Scaling Plot (MDS) of Figure 10. Figure 10 compares the statistical similarity of the samples to one another utilizing an MDS plot with pie diagrams (Generated using the DetritalPy software of Sharman et al. (2018b) and based of methods described in Vermeesch (2018). This change in age pattern is rather abrupt and was likely accomplished within one million years. The zircon REE chemistry data (Figures 7 and 8) suggest that the bulk of the detrital zircon grains in the Cenozoic Molasse strata were primarily derived from magmatic or meta-magmatic rocks. However, after ~22 Ma there appears to have been a slight increase in the input of Variscan and Caledonian metamorphic sources. In the next section, we present a scenario of how this abrupt change can possibly be linked to the tectonic exhumation of the region surrounding the Lepontine Dome, the most likely sediment source for the central Swiss Molasse (Schlunegger et al., 1998; Von Eynatten et al., 1999). This provenance scenario, presented in chronological order, also includes consideration of the apparent first-cycle zircon grains (34 Ma) encountered in the Eocene North Helvetic Flysch. The provenance of the detrital zircon grains is thus discussed within a geodynamic framework of the Alpine orogeny.

8.1 Eocene Drainage Divide During Deposition of the North Helvetic Flysch

The subduction of the European plate beneath the Adriatic plate began in the Late Cretaceous and was associated with the closure of the Tethys and Valais oceans (Schmid et al., 1996). The subducted material mainly included Tethyan oceanic crust, parts of the Valais oceans, and continental crustal slivers of the Briannçonnais or Iberian microcontinent (Schmid et al., 1996; Kissling and Schlunegger, 2018). The introduction of the European plate into the subduction channel resulted in high-pressure metamorphic overprints of these rocks. Subduction of the oceanic crust resulted in the down-warping of the European plate and the formation of the

https://doi.org/10.5194/se-2020-44
Preprint. Discussion started: 29 April 2020

Flysch trough, where clastic turbidites sourced from the erosion of the Adriatic orogenic lid were deposited in a deep-marine trench on the distal European plate (Sinclair et al., 1997). This also includes the volcano-clastic material of the Taveyannaz sandstone (Sinclair et al., 1997; Lu et al., 2018) and the related 34 Ma first-cycle zircon grains encountered in the Eocene North Helvetic Flysch. Hence, while arc magmatism was situation on the Adriatic continental upper plate, volcanoclastic material was shed into the flysch trough on the European continental margin. This implies that during Flysch sedimentation, the N-S drainage divide was likely situated somewhere within the Adriatic upper plate margin.

8.2 Abrupt Oligo-Miocene Detrital Zircon U-Pb Provenance Shift

Between 35 and 32 Ma, buoyant material of the European continental crust entered the subduction channel (Schmid et al., 1996; Handy et al., 2010). Strong tensional forces between the dense and subducted oceanic European lithosphere and the buoyant European continental crust possibly resulted in the break-off of the oceanic plate. As a result, the European plate experienced a phase of rebound and uplift, which was accomplished by back-thrusting along the Periadriatic Lineament (Schmid et al., 1989) and progressive ductile thrusting and duplexing of the deeper Penninic domain (e.g., Wiederkehr et al. 2009; Steck et al., 2013). Although this model has recently been challenged based on zircon U-Pb and Hf isotopic compositions from the Tertiary Periadriatic intrusives (Ji et al., 2018), it still offers the most suitable explanation of the Alpine processes during the Oligocene (Kissling and Schlunegger, 2018). In response, the topographic and drainage divide shifted farther north to the locus of back-thrusting. Streams reestablished their network and eroded the Alpine topography through headward retreat, thereby rapidly eroding and downcutting into deeper crustal levels from the Austroalpine cover nappes and into the Penninic units (Figure 11a; Schlunegger and Norton, 2013). This is indicated by an increase of crystalline clasts in the conglomerates of the Lower Freshwater Molasse (Gasser, 1968; Stürm, 1973) and it is reflected by the detrital zircon U-Pb ages characterized by a cosmopolitan spectra that span the entire spread from Cadomian and older to late Variscan zircon grains (Figure 10).

Surface uplift and progressive erosional unroofing also resulted in a steadily increasing sediment flux into the Molasse basin (Kuhlemann, 2000; Willett and Schlunegger, 2010) and a continuous increase in plutonic and volcanic clasts in the conglomerates (Stürm, 1973; Kempf et

https://doi.org/10.5194/se-2020-44
Preprint. Discussion started: 29 April 2020

Solid Earth Discussions

al., 1999) throughout the Oligocene (Figure 11b). However, this pattern fundamentally changed at ~22-20 Ma when rapid slip along the Simplon fault occurred (Schlunegger and Willett, 1999), resulting in the rapid exhumation of the Lepontine dome as recorded by currently exposed rocks (Figure 11c; Boston et al., 2017). Although thermal modeling and heavy mineral thermochronometric data imply that fastest cooling occurred between ~ 20-15 Ma (Campani et al., 2010; Boston et al., 2017), tectonic exhumation likely started prior to this time interval given the lag time of isotherm perturbations at upper crustal levels (Schlunegger and Willet, 1999). In contrast to Schlunegger et al. (1998), Von Eynatten et al. (1999) suggested, on the basis of detrital mica $^{40}Ar/^{39}Ar$ age patterns, that slip along the Simplon normal fault did not result in a major change of the Alpine drainage organization, and that the Lepontine was still a major sediment source for the Molasse Basin even after the period of rapid updoming and exhumation. In the Lucerne Section, contemporaneous changes included: (i) a shift in the petrographic composition of conglomerates with igneous constituents starting to dominate the clast suite (Schlunegger et al., 1998), (ii) a shift toward predominance of epidote in the heavy mineral spectra (Gasser, 1966), (iii) a continuous decrease in sediment discharge (Kuhlemann, 2000) paired with a fining-upward trend in the 22-20 Ma fluvial sediments of the LFM (Schlunegger et al., 1997a), and (iv) a return from terrestrial (LFM) back to marine (UMM) sedimentation at ~20 Ma within an underfilled flexural foreland basin (Keller, 1989; Garefalakis and Schlunegger, 2019). Our new detrital zircon U-Pb ages exhibit by an abrupt shift towards detrital zircon signatures dominated by Variscan zircons (Figure 10), supporting the notion of erosion of deeper crustal levels in response to tectonic exhumation. Because the Lucerne Section was situated due north of the Lepontine dome, and since this area was a major source of sediment for the Molasse basin even after this phase of rapid tectonic exhumation (Von Eynatten et al., 1999), we consider that these detrital zircon grains were most likely sourced from this part of the Central Alps. The shift to predominantly Variscan zircon grains in UFM deposits is also observed in the western Swiss Molasse Basin (Thun Section; Figure 5 and 10), which hosts conglomerate and sandstone that were derived both from the footwall and the hanging wall of the Simplon detachment fault (Matter, 1964; Schlunegger et al., 1993; Eynatten et al., 1999. A similar related signal was also identified in the axial drainage of the Molasse ~200 km farther east in the submarine Basal Hall Formation (~20 Ma) (Sharman et al., 2018a).

https://doi.org/10.5194/se-2020-44
Preprint. Discussion started: 29 April 2020

8.3 Constrains on surface exhumation of external massifs

It has been suggested that rapid rock uplift of the external Aar Massif (Figure 1), which is in close proximity to the Thun and Lucerne sections, likely started at ~20 Ma (Herwegh et al., 2017; 2019). However, we do not see a related signal in the detrital zircon U-Pb age patterns (Figure 10). Based on geochemical data of detrital garnet, Stutenbecker et al. (2019) showed that the first crystalline material of the Alpine external massifs became exposed to the surface no earlier than ~14 Ma, with the consequence that related shifts were not detected in the zircon age populations. In fact, low-temperature thermochronometric data from the Aar and Mont Blanc Massifs (e.g. Vernon et al., 2009; Glotzbach et al., 2011) document a major exhumation phase of the external massifs in the latest Miocene and early Pliocene, likely related to out-of-sequence thrusting and duplexing at depth. It is therefore likely, that surface exposure of the external massifs might not have occurred until the late Miocene-early Pliocene.

8.4 Continuous detrital-zircon age evolution in eastern Molasse Basin

The detrital zircon ages of the sediments collected in the eastern region of the Swiss Molasse (Bregenz Section; Figure 1 and 3c) show a shift where the relative abundance of Variscan material continuously increased through time (Figures 6 and 10). The material of this region was derived from the eastern Swiss Alps, which includes the Austroalpine units, and possibly the eastern portion of the Lepontine Dome (Kuhlemann and Kempf, 2002). This area was not particularly affected by tectonic exhumation (Schmid et al., 1996). Therefore, we interpret the continuous change in the age populations as record of a rather normal unroofing sequence into the Alpine edifice.

8.5 Tectonic exhumation and relationships to decreasing sediment flux

The overall decrease in sediment discharge, which contributed to the transgression of the Upper Marine Molasse (Garefalakis and Schlunegger, 2019), could be related to the tectonic exhumation of the Lepontine Dome. In particular, slip along the Simplon detachment fault resulted in the displacement of a ca. 10 km-thick stack of rock units within a few million years (Schlunegger and Willett, 1999; Campani et al., 2010). A mechanism such as this is expected to leave a measurable impact on a landscape, which possibly includes (i) a reduction of the overall topography in the region of the footwall rocks (provided not all removal of rock was

https://doi.org/10.5194/se-2020-44
Preprint. Discussion started: 29 April 2020

compensated by uplift), (ii) a modification and thus a perturbation of the landscape morphometry, particularly in the footwall of a detachment fault (Pazzaglia et al., 2007), and (iii) exposure of rock with a higher metamorphic grade and thus a lower bedrock erodibility (Kühni and Pfiffner, 2001). We lack quantitative data to properly identify the main driving force and therefore consider that the combination of these three effects possibly contributed to an overall lower erosional efficiency of the Alpine streams, with the consequence that sediment flux to the Molasse decreased for a few million years. We thus use these mechanisms, together with the larger subsidence (Garefalakis and Schlunegger, 2019), to explain the shallowing-upward fluvial deposition in the post 22 Ma LFM and the transgression of the UMM. Low sediment supply prevailed until steady state erosional conditions were re-established during deposition of the UFM, as implied by the increase in sediment discharge to pre-20 Ma conditions towards the end of the UMM (Kuhlemann, 2000).

9 Conclusions

During deposition of the LFM, at ~22 Ma, detrital zircon U-Pb ages record decreased contributions from Austroalpine cover nappes and erosion into crystalline basement of the Penninic nappes. Erosional mechanisms mainly occurred as normal unroofing process through continuous dissection into the Alpine edifice. The abrupt shift in the age populations of detrital zircon at ~22 Ma reflected in the Central Swiss Molasse indicates a phase of fast tectonic exhumation of the Lepontine Dome. Molasse sediments that were derived from the lateral margin of the Lepontine area (Thun and Bregenz Sections) were less affected by this phase of rapid tectonic exhumation, and age populations record a more continuous unroofing sequence. Tectonic exhumation was associated with a drop in sediment supply to the Molasse, fining upward trends and contributed to the establishment of shallow marine conditions. This could reflect the shift towards a less erosive landscape where tectonic exhumation resulted in a reduction of relief and exposure of rocks with low erodibility.

Data Availability: Due to the nature of the U-Pb and Geochemistry data (LASS and Depth Profiled), the data have been included in a supplemental document and are not uploaded to Geochron.org

https://doi.org/10.5194/se-2020-44
Preprint. Discussion started: 29 April 2020

Supplemental Files:

Supplemental File 1: All depth profiled detrital zircon U-Pb data. (includes Rim-Core distinction that is not allowed on Geochron.org

Supplemental File 2: All Geochemistry data from LASS analysis. This Geochem data also includes the associated ages from Supplemental File 1.

Author Contributions:

OA: As primary author OA collected samples, analyzed samples at UTchron, led the writing of the manuscript, and assembled collaborators.

DS: DS collected a number of the samples, analyzed some samples with JM and AM at the University of Kansas, helped analyze samples at UTchron, and aided in the writing of the manuscript

JM: JM collected a number of the samples with DS, wrote his Master's Thesis at KU on the U-Pb and (U-Th)/He at KU, and aided in the writing of the manuscript.

AM: AM was advisor to JM at KU during his masters work, he analyzed a number of the U-Pb samples at KU, and aided in the writing of the manuscript.

FS: FS helped with sample collection, met for a field trip in Switzerland, provided expertise on the Molasse and Alpine Orogen, and aided in the writing of the manuscript.

Competing Interests: The authors declare that they have no conflict of interest

Acknowledgements

Thanks to the Jackson School of Geoscience at the University of Texas at Austin and to Sonoma State University for financial support. We would like to thank Lisa Stockli and Des Patterson for help with laboratory work at UTChron. Thanks to Andrew Smye, Jeff Marsh, Ryan Mackenzie, and Shannon Loomis and for extensive discussion of the research project.

Table and Figure Captions

Tables

Table 1. Sample Information. Depositional age errors are based on: Lucerne Section- Schlunegger et al. (1997a); Thun Section- Schlunegger et al. (1993; 1996); Bregenz Section- Oberhauser (1994), Kempf et al. (1999), and Schaad et al. (1992). 'X' in 'U-Pb' and 'Geochem'

https://doi.org/10.5194/se-2020-44
Preprint. Discussion started: 29 April 2020

columns indicate data available for that sample. Final column indicates if samples were analyzed at either the University of Kansas (KU) or the University of Texas at Austin (UT). Errors for depositional ages are discussed in Section 3. Corresponding methods are found in the Section 4.

Figures

Figure 1. Geologic map of the Central Alps and Swiss Molasse Basin highlighting geologic features and paleogeographic units discussed in the text (map is adapted from Garefalakis and Schlunegger (2019) and based on: Froitzheim et al. (1996), Schmid et al. (2004), Handy et al. (2010), and Kissling and Schlunegger (2018). Locations are shown for the Lucerne Section, Thun Section, and Bregenz Section that are highlighted in Figures 3a, 3b, and 3c, respectively.

Figure 2. Generalized stratigraphy of the Molasse Basin. Modified from Miller (2009) and (Keller, 2000).

Figure 3. Stratigraphic units and sample locations of the three sampled sections A) Lucerne Section: geologic map and cross section modified from (Schlunegger et al., 1997a). In both the map and the simplified cross section, sample numbers are only the last two digits of the sample numbers from Table 1. B) Thun Section: geologic map modified from Schlunegger et al. (1993; 1996). C) Bregenz Section: geologic map simplified from Oberhauser, (1994), Kempf et al., (1999), and Schaad et al. (1992).

Figure 4. Detrital zircon U-Pb age data from the Lucerne Section (locations of samples depicted in Figure 3a) plotted as Kernel Density Estimations (KDE; Bandwidth set to 10), a Cumulative Distribution Plot (CDP), and as pie diagrams. Colored bars in the KDE and colored wedges in the pie diagrams show the relative abundance of age groups discussed in Section 5. Samples associated with each unit are referenced in Table 1. Plot only shows ages from 0-1000 Ma; however, a small number of older ages were analyzed and that data can be found in Supplemental File 1. N= (Number of samples, number of ages depicted/ total number of total ages).

https://doi.org/10.5194/se-2020-44
Preprint. Discussion started: 29 April 2020

Figure 5. Detrital zircon U-Pb age data from the Thun Section (locations of samples depicted in Figure 3b). See Figure 4 legend and caption for additional information.

Figure 6. Detrital zircon U-Pb age data from the Bregenz Section (locations of samples depicted in Figure 3c). See Figure 4 legend and caption for additional information.

Figure 7. Detrital zircon Rare Earth Element (REE) spider diagram for samples collected from the Lucerne Section. (A) Variscan U-Pb ages and REE data for samples younger than a 22 Ma depositional age and (B) older than a 22 Ma depositional age. (C) Caledonian and Cadomian U-Pb ages and REE data for samples younger than a 22 Ma depositional age and (D) older than a 22 Ma depositional age. For plots A and C the geochemical data is drawn from samples SFB33 (21 Ma), SFB49 (19Ma). SFB14 (17.5 Ma), and SFB38 (13.5 Ma). For B and D the geochemical data is drawn from samples SFB21 (22.5 Ma) and SFB45 (27 Ma). The data suggest that detrital zircons from all three recent orogenic cycles record primarily grains that are magmatic in origin (Belousova et al., 2002; Hoskin and Ireland, 2000), with little evidence of metamorphic/metasomatic grains. Data can be found in Supplemental File 2.

Figure 8. Age vs U/Th comparison for detrital zircon grains with depositional ages older than 22 Ma and younger than 22 Ma. A) Variscan aged grains, B) Caledonian and Cadomian age grains. Although not definitive, grains with elevated U/Th (or low Th/U; e.g. Rubatto et al. 2002) have a higher likelihood of being metamorphic in origin. There are few Variscan grains with elevated U/Th from both the pre- and post-22 Ma depositional ages, suggesting little input of metamorphic sources for these ages. There are a large number of Caledonian and a handful of Cadomian grains with elevated U/Th from both the pre- and post-22 Ma depositional ages, indicating metamorphic sources for these age grains are prevalent.

Figure 9. Rim vs core ages for detrital zircon grains from samples with depositional ages older than 22 Ma and younger than 22 Ma from the Lucerne Section. Prior to the 22 Ma transition in source area there is a minor number of Variscan rims on Cadomian and Caledonian cores. In

https://doi.org/10.5194/se-2020-44
Preprint. Discussion started: 29 April 2020

samples younger than 22 Ma there is a noticeable increase in Variscan rims on Caledonian, Cadomian, and Proterozoic cores. Error bars are 2 sigma non-propagated errors.

Figure 10. Multidimensional Scaling Plot (MDS) of detrital zircon U-Pb ages for all units from the Molasse Basin. The MDS plot was produced with the DetritalPy software of Sharman et al. (2018b) and is based on methods outlined by Vermeesch (2018). Pie diagram colors correspond to age groups from Figure 4 and ages discussed in Section 4.

Figure 11. Schematic cross-section through the central Alps of Switzerland, illustrating the development of the Alpine relief and the topography through time. A) 30 Ma-25 Ma: Slab breakoff resulted in backthrusting along the Periadriatic fault and in the growth of the Alpine topography. The erosional hinterland was mainly made up of the Austroalpine cover nappes (Adriatic plate) and Penninic sedimentary rocks at the orogen front. B) 25 Ma: Ongoing surface erosion resulted in the formation of an Alpine-type landscape with valleys and mountains. First dissection into the crystalline core of the European continental plate was registered by the first arrival of Penninc crystalline material in the foreland basin sometime between 25 and 22 Ma, depending on the location within the basin. 22 Ma was also the time when sediment discharge to the Molasse was highest. Tectonic exhumation through slip along the Simplon fault started to occur at the highest rates. C) 20 Ma: Tectonic exhumation along the Simplon fault resulted in widespread exposure of high-grade rocks, in a shift in the clast suites of the conglomerates and in a change in the detrital zircon age signatures. Faulting along the detachment fault most likely subdued the topography in the hinterland. As a result, sediment flux to the Molasse basin decreased, and the basin became underfilled and was occupied by the peripheral sea of the Upper Marine Molasse. (Figures based on restored sections by Schlunegger and Kissling, 2015).

References

Allen P.A., Mange-Rajetzky M., Matter A., Homewood P.: Dynamic palaeogeography of the open Burdigalian seaway, Swiss Molasse basin. Eclogae Geol. Helv., 78, 351–381, 1985.

Allen, M., Saville, C., Blanc, E. P., Talebian, M., and Nissen, E.: Orogenic plateau growth: Expansion of the Turkish-Iranian Plateau across the Zagros fold-and-thrust belt, Tectonics, 32, 171-190, 2013.

https://doi.org/10.5194/se-2020-44
Preprint. Discussion started: 29 April 2020

Solid Earth Discussions

Allen, P. A., Crampton, S. L., and Sinclair, H. D.: The inception and early evolution of the North Alpine Foreland Basin, Switzerland, Basin Research, 3, 143-163, 1991.

Andersen, T.: Correction of common lead in U–Pb analyses that do not report 204Pb, Chemical geology, 192, 59-79, 2002.

Anfinson, O. A., Malusà, M. G., Ottria, G., Dafov, L. N., and Stockli, D. F.: Tracking coarse-grained gravity flows by LASS-ICP-MS depth-profiling of detrital zircon (Aveto Formation, Adriatic foredeep, Italy), Mar Petrol Geol, 77, 1163-1176, 2016.

Barber, D. E., Stockli, D. F., and Galster, F.: The Proto-Zagros Foreland Basin in Lorestan, Western Iran: Insights From Multimineral Detrital Geothermochronometric and Trace Elemental Provenance Analysis, Geochemistry, Geophysics, Geosystems, 20, 2657-2680, 2019.

Beck, P. und Rutsch, R. F.: Geol. Atlasblatt 21 (1:25,000) Münsingen—Konolfingen—Gerzensee—Heimberg, Schweiz. Geol. Komm, 1949.

Bell, E. A., Boehnke, P., Barboni, M., and Harrison, T. M.: Tracking chemical alteration in magmatic zircon using rare earth element abundances, Chemical Geology, 510, 56-71, 2019.

Belousova, E., Griffin, W. L., O'Reilly, S. Y., and Fisher, N.: Igneous zircon: trace element composition as an indicator of source rock type, Contributions to mineralogy and petrology, 143, 602-622, 2002.

Boston, K. R., Rubatto, D., Hermann, J., Engi, M., and Amelin, Y.: Geochronology of accessory allanite and monazite in the Barrovian metamorphic sequence of the Central Alps, Switzerland, Lithos, 286, 502-518, 2017.

Büchi, U. P., and Schlanke, S.: Zur paläogeographie der schweizerischen Molasse, Erdöl-Erdgas-Zeitschrift, 93, 57-69, 1977.

Burkhard, M., and Sommaruga, A.: Evolution of the western Swiss Molasse basin: structural relations with the Alps and the Jura belt, Geological Society, London, Special Publications, 134, 279-298, 1998.

Bütler, E., Winkler, W., and Guillong, M.: Laser ablation U/Pb age patterns of detrital zircons in the Schlieren Flysch (Central Switzerland): new evidence on the detrital sources, Swiss Journal of Geosciences, 104, 225, 2011.

Campani, M., Herman, F., and Mancktelow, N.: Two-and three-dimensional thermal modeling of a low-angle detachment: Exhumation history of the Simplon Fault Zone, central Alps, Journal of Geophysical Research: Solid Earth, 115, 2010.

https://doi.org/10.5194/se-2020-44
Preprint. Discussion started: 29 April 2020

Cederbom, C. E., Sinclair, H. D., Schlunegger, F., and Rahn, M. K.: Climate-induced rebound and exhumation of the European Alps, Geology, 32, 709-712, 2004.

Cederbom, C. E., Van Der Beek, P., Schlunegger, F., Sinclair, H. D., and Oncken, O.: Rapid extensive erosion of the North Alpine foreland basin at 5–4 Ma, Basin Research, 23, 528-550, 2011.

Crampton, S., and Allen, P.: Recognition of forebulge unconformities associated with early stage foreland basin development: example from the North Alpine Foreland Basin, AAPG bulletin, 79, 1495-1514, 1995.

D'Lemos, R., Strachan, R., and Topley, C.: The Cadomian orogeny in the North Armorican Massif: a brief review, Geological Society, London, Special Publications, 51, 3-12, 1990.

Davis, J. H., and Blanckenburg, F.: Slab breakoff: A model of lithosphere detachment and its test in the magmatism and deformation of collisional orogens, Earth and Planetary Science Letters, 129, 85-102, 1995.

DeCelles, P. G., and Giles, K. A.: Foreland basin systems, Basin research, 8, 105-123, 1996.

Dewey, J., and Horsfield, B.: Plate tectonics, orogeny and continental growth, Nature, 225, 521-525, 1970.

Diem, B.: Die Untere Meeresmolasse zwischen der Saane (Westschweiz) und der Ammer (Oberbayern), Eclogae Geol Helv, 79, 493-559, 1986.

Dietrich, V.: Die Oberhalbsteiner Talbildung im Tertiär: ein Vergleich zwischen den Ophiolithen und deren Detritus in der ostschweizerischen Molasse, Geologisches Institut der Eidg. Technischen Hochschule und der Universität, 1969.

Dunkl, I., Mikes, T., Frei, D., Gerdes, A., von Eynatten, H.: PepiAGE data reduction program for time-resolved U/Pb analyses – introduction and call for tests and discussion. University of Goettingen Publication, p. 15, 2009.

Engesser, B., and Mayo, N. A.: A biozonation of the Lower Freshwater Molasse (Oligocene and Agenian) of Switzerland and Savoy on the basis of fossil mammals., Münchner Geowiss, 10, 67-84, 1987.

https://doi.org/10.5194/se-2020-44
Preprint. Discussion started: 29 April 2020

Engi, M., Todd, C., and Schmatz, D.: Tertiary metamorphic conditions in the eastern Lepontine Alps, Schweizerische Mineralogische und Petrographische Mitteilungen, 75, 347-369, 1995.

Engi, M., Bousquet, R., and Berger, A.: Explanatory notes to the map: Metamorphic structure of the Alps-Central Alps, Mitteilungen der Österreichischen Mineralogischen Gesellschaft, 149, 157-173, 2004.

Finger, F., Roberts, M., Haunschmid, B., Schermaier, A., and Steyrer, H.-P.: Variscan granitoids of central Europe: their typology, potential sources and tectonothermal relations, Mineralogy and Petrology, 61, 67-96, 1997.

Franke, W.: The Variscan orogen in Central Europe: construction and collapse, Geological Society, London, Memoirs, 32, 333-343, 2006.

Frey, M., Teichmiiller, M., Teichmiiller, R., Mullis, J., Kfinzi, B., Breitschmid, A., Gruner, U., and Schwitzer, B.; Very low grade metamorphism in external parts of the Central Alps: Illite crystallinity, coal rank and fluid inclusion data, Eclogae Geol. Helv., 73, 173-203, 1980.

Froitzheim, N., Schmid, S. M., and Frey, M.: Mesozoic paleogeography and the timing of eclogite-facies metamorphism in the Alps: a working hypothesis, Eclogae Geol Helv, 89, 81-&, 1996.

Fry, B., Deschamps, F., Kissling, E., Stehly, L., and Giardini, D.: Layered azimuthal anisotropy of Rayleigh wave phase velocities in the European Alpine lithosphere inferred from ambient noise, Earth and Planetary Science Letters, 297, 95-102, 2010.

Fuchtbauer, H.: Sedimentpetrographische Untersuchungen in der alteren Molasse nordlich der Alpen, Eclogae Geol. Helv., 57, 157-298, 1964.

Garefalakis, P., and Schlunegger, F.: Stratigraphic architecture of the Upper Marine Molasse implies incipient westward tilt of the foreland plate, Poster GeoBonn, 2018.

Gasser, U.: Sedimentologische Untersuchungen in der äusseren Zone der subalpinen Molasse des Entlebuchs (Kt. Luzern), Verlag nicht ermittelbar, 1966.

Gasser, U.: Die innere Zone der subalpinen Molasse des Entlebuchs (Kt. Luzern): Geologie und Sedimentologie, Birkhäuser, 1968.

https://doi.org/10.5194/se-2020-44
Preprint. Discussion started: 29 April 2020

Solid Earth Discussions

Gebauer, D.: Alpine geochronology of the Central and Western Alps: new constraints for a complex geodynamic evolution, Schweizerische Mineralogische und Petrographische Mitteilungen, 79, 191-208, 1999.

Glotzbach, C., Van Der Beek, P. A., and Spiegel, C.: Episodic exhumation and relief growth in the Mont Blanc massif, Western Alps from numerical modelling of thermochronology data, Earth and Planetary Science Letters, 304, 417-430, 2011.

Grasemann, B., and Mancktelow, N. S.: Two-dimensional thermal modelling of normal faulting: the Simplon Fault Zone, Central Alps, Switzerland, Tectonophysics, 225, 155-165, 1993.

Grimes, C., Wooden, J., Cheadle, M., and John, B.: "Fingerprinting" tectono-magmatic provenance using trace elements in igneous zircon, Contributions to Mineralogy and Petrology, 170, 46, 2015.

Habicht, K.: Neuere Beobachtungen in der subalpinen Molasse zwischen Zugersee und dem st. gallischen Rheintal, Geologisches Institut der Eidg. Technischen Hochschule und der Universität, 1945.

Handy, M. R., Schmid, S. M., Bousquet, R., Kissling, E., and Bernoulli, D.: Reconciling plate-tectonic reconstructions of Alpine Tethys with the geological–geophysical record of spreading and subduction in the Alps, Earth-Science Reviews, 102, 121-158, 2010.

Herwegh, M., Berger, A., Baumberger, R., Wehrens, P., and Kissling, E.: Large-scale crustal-block-extrusion during late Alpine collision, Scientific reports, 7, 1-10, 2017.

Herwegh, M., Berger, A., Glotzbach, C., Wangenheim, C., Mock, S., Wehrens, P., Baumberger, R., Egli, D., and Kissling, E.: Late stages of continent-continent collision: Timing, kinematic evolution, and exhumation of the Northern rim (Aar Massif) of the Alps, Earth-science reviews, 102959, 2019.

Hetényi, G., Molinari, I., Clinton, J., Bokelmann, G., Bondár, I., Crawford, W. C., Dessa, J.-X., Doubre, C., Friederich, W., and Fuchs, F.: The AlpArray seismic network: a large-scale European experiment to image the Alpine Orogen, Surveys in geophysics, 39, 1009-1033, 2018.

Homewood, P., Allen, P., and Williams, G.: Dynamics of the Molasse Basin of western Switzerland, in: Foreland basins, Spec. Publ. Int. Ass. Sediment, 199-217, 1986.

Hoskin, P. W., and Ireland, T. R.: Rare earth element chemistry of zircon and its use as a provenance indicator, Geology, 28, 627-630, 2000.

https://doi.org/10.5194/se-2020-44
Preprint. Discussion started: 29 April 2020

Hoskin, P. W.: Trace-element composition of hydrothermal zircon and the alteration of Hadean zircon from the Jack Hills, Australia, Geochimica et Cosmochimica Acta, 69, 637-648, 2005.

Hunziker, J. C., Desmons, J., and Hurford, A. J.: Thirty-two years of geochronological work in the Central and Western Alps: a review on seven maps, 1992.

Hurford, A. J.: Cooling and uplift patterns in the Lepontine Alps South Central Switzerland and an age of vertical movement on the Insubric fault line Contributions to Mineralogy and Petrology, 92, 413-427, 1986.

Jin, J., Aigner, T., Luterbacher, H., Bachmann, G. H., and Müller, M.: Sequence stratigraphy and depositional history in the south-eastern German Molasse Basin, Mar Petrol Geol, 12, 929-940, 1995.

Jordan, T., and Flemings, P. B.: Large-scale stratigraphic architecture, eustatic variation, and unsteady tectonism: a theoretical evaluation, Journal of Geophysical Research: Solid Earth, 96, 6681-6699, 1991.

Jost, J., Kempf, O., and Kälin, D.: Stratigraphy and palaeoecology of the Upper Marine Molasse (OMM) of the central Swiss Plateau, Swiss Journal of Geosciences, 109, 149-169, 2016.

Kälin, D., and Kempf, O.: High-resolution stratigraphy from the continental record of the Middle Miocene Northern Alpine Foreland Basin of Switzerland, Neues Jahrbuch für Geologie und Paläontologie-Abhandlungen, 254, 177-235, 2009.

Keller, B.: Fazies und Stratigraphie der Oberen Meeresmolasse (Unteres Miozän) zwischen Napf und Bodensee. Unpubl. PhD Thesis, Universität Bern, Bern, 402 p, 1989.

Keller, B.: Fazies der Molasse anhand eines Querschnitts durch das zentrale Schweizer Mittelland, Jber. Mitt. Oberrhein, 82, 55-92, 2000.

Kempf, O., Matter, A., Burbank, D., and Mange, M.: Depositional and structural evolution of a foreland basin margin in a magnetostratigraphic framework: the eastern Swiss Molasse Basin, International Journal of Earth Sciences, 88, 253-275, 1999.

Kissling, E., and Schlunegger, F.: Rollback orogeny model for the evolution of the Swiss Alps, Tectonics, 37, 1097-1115, 2018.

Krawczyk, C., McCann, T., Cocks, L.R.M., England, R.W., McBride, J.H. and Wybraniec, S.: Caledonian tectonics, In The Geology of Central Europe (McCann, T., Ed.), 1, Precambrian and Paleozoic, Geological Society, London, 303-381, 2008.

https://doi.org/10.5194/se-2020-44
Preprint. Discussion started: 29 April 2020

Solid Earth Discussions

Kuhlemann, J.: Post-collisional sediment budget of circum-Alpine basins (Central Europe), Mem. Sci. Geol. Padova, 52, 1-91, 2000.

Kuhlemann, J., and Kempf, O.: Post-Eocene evolution of the North Alpine Foreland Basin and its response to Alpine tectonics, Sedimentary Geology, 152, 45-78, 2002.

Kühni, A., and Pfiffner, O.-A.: Drainage patterns and tectonic forcing: a model study for the Swiss Alps, Basin Research, 13, 169-197, 2001.

Kylander-Clark, A. R. C., Hacker, B. R., and Cottle, J. M.: Laser-ablation split-stream ICP petrochronology, Chemical Geology, 345, 99-112, 10.1016/j.chemgeo.2013.02.019, 2013.

Laubscher, H.: Detachment, shear, and compression in the central Alps, Geol. Soc. Am. Mem, 158, 191-211, 1983.

Lihou, J. C., and Allen, P. A.: Importance of inherited rift margin structures in the early North Alpine Foreland Basin, Switzerland, Basin Research, 8, 425-442, 1996.

Lippitsch, R., Kissling, E., and Ansorge, J.: Upper mantle structure beneath the Alpine orogen from high-resolution teleseismic tomography, Journal of Geophysical Research: Solid Earth, 108, 2003.

Lu, G., Winkler, W., Rahn, M., von Quadt, A., and Willett, S. D.: Evaluating igneous sources of the Taveyannaz formation in the Central Alps by detrital zircon U–Pb age dating and geochemistry, Swiss Journal of Geosciences, 111, 399-416, 2018.

Mair, D., Lechmann, A., Herwegh, M., Nibourel, L., and Schlunegger, F.: Linking Alpine deformation in the Aar Massif basement and its cover units–the case of the Jungfrau–Eiger mountains (Central Alps, Switzerland), Solid Earth, 9, 1099-1122, 2018.

Malusa, M. G., Anfinson, O. A., Dafov, L. N., and Stockli, D. F.: Tracking Adria indentation beneath the Alps by detrital zircon U-Pb geochronology: Implications for the Oligocene-Miocene dynamics of the Adriatic microplate, Geology, 44, 155-158, 10.1130/G37407.1, 2016.

Mancktelow, N.: The Simplon Line: a major displacement zone in the western Lepontine Alps, Eclogae Geol Helv, 78, 73-96, 1985.

Mancktelow, N. S., and Grasemann, B.: Time-dependent effects of heat advection and topography on cooling histories during erosion, Tectonophysics, 270, 167-195, 1997.

https://doi.org/10.5194/se-2020-44
Preprint. Discussion started: 29 April 2020

Marsh, J. H., and Stockli, D. F.: Zircon U–Pb and trace element zoning characteristics in an anatectic granulite domain: Insights from LASS-ICP-MS depth profiling, Lithos, 239, 170-185, 2015.

Matter, A.: Sedimentologische Untersuchungen im östlichen Napfgebiet (Entlebuch—Tal der Grossen Fontanne, Kt. Luzern): Eclogae Geologicae Helvetiae, 57, 315–428, 1964.

Matter, A., Homewood, P. W., Caron, C., Van Stuijvenberg, J., Weidmann, M., and Winkler, W.: Flysch and molasse of central and western Switzerland, in Trümpy, R., ed., Geology of Switzerland, a guide book: Schweiz Geologica Kommissione, 261–293, 1980.

Mazurek, M., Hurford, A. J., and Leu, W.: Unravelling the multi-stage burial history of the Swiss Molasse Basin: integration of apatite fission track, vitrinite reflectance and biomarker isomerisation analysis, Basin Research, 18, 27-50, 2006.

McCann, T. (Ed.): The geology of central Europe, Geol. Soc. London, 2008.

Müller, B., Schaltegger, U., Klötzli, U., and Flisch, M.: Early Cambrian oceanic plagiogranite in the Silvretta nappe, eastern Alps: Geochemical, zircon U-Pb and Rb-Sr data from garnet-hornblende-plagioclase gneisses, Geologische Rundschau, 85, 822-831, 1996.

Neubauer, F.: Evolution of late Neoproterozoic to early Paleozoic tectonic elements in Central and Southeast European Alpine mountain belts: review and synthesis, Tectonophysics, 352, 87-103, 2002.

Niggli, E., and Niggli, C.: Karten der Verbreitung einiger Mineralien der alpidischen Metamorphose in den Schweizer Alpen (Stilpnomelan, Alkali-Amphibol, Chloritoid, Staurolith, Disthen, Sillimanit), Eclogae Geol Helv, 58, 335-368, 1965.

Oberhauser, R.: 110 St. Galen Nord Und 111 Dornbern Nord, Geologische Bundesanstalt, Vienna, AT, 1994.

Paton, C., Hellstrom, J., Paul, B., Woodhead, J., and Hergt, J.: Iolite: Freeware for the visualisation and processing of mass spectrometric data, Journal of Analytical Atomic Spectrometry, 26, 2508-2518, 2011.

Pazzaglia, F. J., Selverstone, J., Roy, M., Steffen, K., Newland-Pearce, S., Knipscher, W., and Pearce, J.: Geomorphic expression of midcrustal extension in convergent orogens, Tectonics, 26, 2007.

https://doi.org/10.5194/se-2020-44
Preprint. Discussion started: 29 April 2020

Solid Earth Discussions
Open Access

Petrus, J. A., and Kamber, B. S.: VizualAge: A Novel Approach to Laser Ablation ICP-MS U-Pb Geochronology Data Reduction, Geostandards and Geoanalytical Research, 36, 247-270, 10.1111/j.1751-908X.2012.00158.x, 2012.

Pfiffner, O.-A., Schlunegger, F., and Buiter, S.: The Swiss Alps and their peripheral foreland basin: Stratigraphic response to deep crustal processes, Tectonics, 21, 3-1-3-16, 2002.

Pfiffner, O. A.: Evolution of the north Alpine foreland basin in the Central Alps, Foreland basins, 219-228, 1986.

Pfiffner, O. A.: Geology of the Alps, John Wiley & Sons, 2014.

Platt, N. H., and Keller, B.: Distal alluvial deposits in a foreland basin setting—the Lower Freshwater Miocene), Switzerland: sedimentology, architecture and palaeosols, Sedimentology, 39, 545-565, 1992.

Rahn, M., Mullis, J., Erdelbrock, K., and Frey, M.: Very low-grade metamorphism of the Taveyanne greywacke, Glarus Alps, Switzerland, Journal of Metamorphic Geology, 12, 625-641, 1994.

Reichenwallner, S.: Die vulkanische Aktivität in den Westalpen hergeleitet aus detritischem Amphibol und Klinopyroxen im Taveyannaz-Sandstein, unpublished Ms thesis, University of Bern, Bern, 57 pp., 2019.

Renz, H.: Die subalpine Molasse zwischen Aare und Rhein, 1937.

Ring, U.: The Alpine geodynamic evolution of Penninic nappes in the eastern Central Alps: geothermobarometric and kinematic data, Journal of Metamorphic Geology, 10, 33-53, 1992.

Rubatto, D.: Zircon trace element geochemistry: partitioning with garnet and the link between U–Pb ages and metamorphism, Chemical geology, 184, 123-138, 2002.

Rubatto, D., Regis, D., Hermann, J., Boston, K., Engi, M., Beltrando, M., and McAlpine, S. R.: Yo-yo subduction recorded by accessory minerals in the Italian Western Alps, Nature Geoscience, 4, 338-342, 2011.

Schaad W., Keller, B., and Matter A.: Die Obere Meeresmolasse (OMM) am Pfänder: Beispiel eines Gilbert-Deltakomplexes, Eclogae Geol. Helv., 85, 145–168, 1992.

Schaltegger, U.: Unravelling the pre-Mesozoic history of Aar and Gotthard massifs (Central Alps) by isotopic dating: a review: The pre-Alpine crustal evolution of the Aar-, Gotthard-and Tavetsch massifs, Schweizerische Mineralogische und Petrographische Mitteilungen, 74, 41-51, 1994.

Schaltegger, U., and Gebauer, D.: Pre-Alpine geochronology of the central, western and southern Alps, Schweizerische Mineralogische und Petrographische Mitteilungen, 79, 79-87, 1999.

Schaltegger, U., Abrecht, J., and Corfu, F.: The Ordovician orogeny in the Alpine basement: constraints from geochronology and geochemistry in the Aar Massif (Central Alps), Swiss Bulletin of Mineralogy and Petrology, 83, 183-239, 2003.

Schegg, R., Cornford, C., and Leu, W.: Migration and accumulation of hydrocarbons in the Swiss Molasse Basin: implications of a 2D basin modeling study, Mar Petrol Geol, 16, 511-531, 1999.

Schlanke, S.: Geologie Der Subalpinen Molasse Zwischen Biberbrugg SZ, Huetten ZH Und Agerisee ZG, Schweiz, 1974.

Schlunegger, F., Matter, A., and Mange, M. A.: Alluvial fan sedimentation and structure of the southern Molasse basin margin, Lake Thun area, Switzerland, Eclogae Geol. Helv., 86, 717–750, 1993.

Schlunegger, F., Burbank, D. W., and Matter, A.: Magnetostratigraphic calibration of the Oligocence to Middle Miocene (30-15 Ma) mammal biozones and depositional sequences of the Swiss Molasse Basin, Eclogae Geol Helv, 89, 753-788, 1996.

Schlunegger, F., Matter, A., Burbank, D. W., and Klaper, E. M.: Magnetostratigraphic constraints on relationships between evolution of the central Swiss Molasse basin and Alpine orogenic events, Geological Society of America Bulletin, 102, 225-241, 1997a.

Schlunegger, F., Leu, W., and Matter, A.: Sedimentary sequences, seismic facies, subsidence analysis, and evolution of the Burdigalian Upper Marine Molasse Group, central Switzerland, AAPG bulletin, 81, 1185-1207, 1997b.

Schlunegger, F., Matter, A., Burbank, D., Leu, W., Mange, M., and Matyas, J.: Sedimentary sequences, seismofacies and evolution of depositional systems of the Oligo/Miocene Lower Freshwater Molasse Group, Switzerland, Basin Research, 9, 1-26, 1997c.

Schlunegger, F., Slingerl, R., and Matter, A.: Crustal thickening and crustal extension as controls on the evolution of the drainage network of the central Swiss Alps between 30 Ma and

https://doi.org/10.5194/se-2020-44
Preprint. Discussion started: 29 April 2020

the present: constraints from the stratigraphy of the North Alpine Foreland Basin and the structural evolution of the Alps, Basin Research, 10, 197-212, 1998.

Schlunegger, F., and Willett, S.: Spatial and temporal variations in exhumation of the central Swiss Alps and implications for exhumation mechanisms, Geological Society, London, Special Publications, 154, 157-179, 1999.

Schlunegger, F., Rieke-Zapp, D., and Ramseyer, K.: Possible environmental effects on the evolution of the Alps-Molasse Basin system, Swiss Journal of Geosciences, 100, 383-405, 10.1007/s00015-007-1238-9, 2007.

Schlunegger, F., and Norton, K. P.: Water versus ice: The competing roles of modern climate and Pleistocene glacial erosion in the Central Alps of Switzerland, Tectonophysics, 602, 370-381, 2013.

Schlunegger, F., and Kissling, E.: Slab rollback orogeny in the Alps and evolution of the Swiss Molasse basin, Nature communications, 6, 1-10, 2015.

Schlunegger, F., and Castelltort, S.: Immediate and delayed signal of slab breakoff in Oligo/Miocene Molasse deposits from the European Alps, Scientific reports, 6, 31010, 2016.

Schmid, S., Aebli, H., Heller, F., and Zingg, A.: The role of the Periadriatic Line in the tectonic evolution of the Alps, Geological Society, London, Special Publications, 45, 153-171, 1989.

Schmid, S. M., Pfiffner, O. A., Froitzheim, N., Schönborn, G., and Kissling, E.: Geophysical-geological transect and tectonic evolution of the Swiss-Italian Alps, Tectonics, 15, 1036-1064, 10.1029/96tc00433, 1996.

Schmid, S. M., Fugenschuh, B., Kissling, E., and Schuster, R.: Tectonic map and overall architecture of the Alpine orogen, Eclogae Geol Helv, 97, 93-117, 10.1007/s00015-004-1113-x, 2004.

Sharman, G. R., Hubbard, S. M., Covault, J. A., Hinsch, R., Linzer, H. G., and Graham, S. A.: Sediment routing evolution in the North Alpine Foreland Basin, Austria: interplay of transverse and longitudinal sediment dispersal, Basin Research, 30, 426-447, 2018a.

Sharman, G. R., Sharman, J. P., and Sylvester, Z.: detritalPy: A Python-based toolset for visualizing and analysing detrital geo-thermochronologic data, The Depositional Record, 4, 202-215, 2018b.

https://doi.org/10.5194/se-2020-44
Preprint. Discussion started: 29 April 2020

Sinclair, H., and Allen, P.: Vertical versus horizontal motions in the Alpine orogenic wedge: stratigraphic response in the foreland basin, Basin Research, 4, 215-232, 1992.

Sinclair, M. R., Wratt, D. S., Henderson, R. D., and Gray, W. R.: Factors affecting the distribution and spillover of precipitation in the Southern Alps of New Zealand—A case study, Journal of Applied Meteorology, 36, 428-442, 1997.

Soto-Kerans, G. M., Stockli, D. F., Janson, X., Lawton, T. F., and Covault, J. A.: Orogen proximal sedimentation in the Permian foreland basin, Geosphere, 2020.

Spicher, A.: Tektonische Karte der Schweiz: 1: 500 000, Schweizerische Geologische Kommission Bern, 1980.

Spiegel, C., Siebel, W., Kuhlemann, J., and Frisch, W.: Toward a comprehensive provenance analysis: A multi-method approach and its implications for the evolution of the Central Alps, SPECIAL PAPERS-GEOLOGICAL SOCIETY OF AMERICA, 37-50, 2004.

Stampfli, G. M., and Borel, G. D.: A plate tectonic model for the Paleozoic and Mesozoic constrained by dynamic plate boundaries and restored synthetic oceanic isochrons, Earth and Planetary Science Letters, 196, 17-33, Doi 10.1016/S0012-821x(01)00588-X, 2002.

Steck, A., Della Torre, F., Keller, F., Pfeifer, H.-R., Hunziker, J., and Masson, H.: Tectonics of the Lepontine Alps: ductile thrusting and folding in the deepest tectonic levels of the Central Alps, Swiss Journal of Geosciences, 106, 427-450, 2013.

Steiger, R. H., and Jäger, E.: Subcommission on geochronology: convention on the use of decay constants in geo-and cosmochronology, Earth and planetary science letters, 36, 359-362, 1977.

Stephan, T., Kroner, U., Romer, R. L., and Rösel, D.: From a bipartite Gondwana shelf to an arcuate Variscan belt: The early Paleozoic evolution of northern Peri-Gondwana, Earth-science reviews, 2019.

Strunck, P., and Matter, A.: Depositional evolution of the western Swiss Molasse, Eclogae Geol Helv, 95, 197-222, 2002.

Stürm, B.: Die Rigischüttung. Sedimentpetrographie, Sedimentologie, Paläogeographie, Tektonik [Ph.D. dissert.], Zürich, Switzerland, Universität Zürich, 98 p., 1973.

Stutenbecker, L., Tollan, P. M., Madella, A., and Lanari, P.: Miocene basement exhumation in the Central Alps recorded by detrital garnet geochemistry in foreland basin deposits, Solid Earth, 10, 1581-1595, 2019.

https://doi.org/10.5194/se-2020-44
Preprint. Discussion started: 29 April 2020

Trümpy, R., Aubert, D., and Bernoulli, D.: Geology of Switzerland: Geological excursions, Wepf, 1980.

Vermeesch, P.: How many grains are needed for a provenance study?, Earth and Planetary Science Letters, 224, 441-451, 10.1016/j.epsl.2004.05.037, 2004.

Vermeesch, P.: Dissimilarity measures in detrital geochronology, Earth-Science Reviews, 178, 310-321, 2018.

Vernon, A. J., van der Beek, P. A., and Sinclair, H. D.: Spatial correlation between long-term exhumation rates and present-day forcing parameters in the western European Alps, Geology, 37, 859-862, 2009.

Von Eynatten, H., Schlunegger, F., Gaupp, R., and Wijbrans, J. R.: Exhumation of the Central Alps: evidence from 40Ar/39Ar laserprobe dating of detrital white micas from the Swiss Molasse Basin, Terra Nova, 11, 284-289, 1999.

Von Eynatten, H., and Wijbrans, J.: Precise tracing of exhumation and provenance using 40Ar/39Ar geochronology of detrital white mica: the example of the Central Alps, Geological Society, London, Special Publications, 208, 289-305, 2003.

von Eynatten, H., and Dunkl, I.: Assessing the sediment factory: the role of single grain analysis, Earth-Science Reviews, 115, 97-120, 2012.

von Raumer, J.: The Palaeozoic evolution in the Alps: from Gondwana to Pangea, Geologische Rundschau, 87, 407-435, 1998.

von Raumer, J. F., Stampfli, G. M., Borel, G., and Bussy, F.: Organization of pre-Variscan basement areas at the north-Gondwanan margin, International Journal of Earth Sciences, 91, 35-52, 10.1007/s005310100200, 2002.

von Raumer, J. F., Stampfli, G. M., and Bussy, F.: Gondwana-derived microcontinents—the constituents of the Variscan and Alpine collisional orogens, Tectonophysics, 365, 7-22, 2003.

von Raumer, J. F., Bussy, F., and Stampfli, G. M.: The Variscan evolution in the External massifs of the Alps and place in their Variscan framework, Comptes Rendus Geoscience, 341, 239-252, 2009.

Wiederkehr, M., Sudo, M., Bousquet, R., Berger, A., and Schmid, S. M.: Alpine orogenic evolution from subduction to collisional thermal overprint: The 40Ar/39Ar age constraints from the Valaisan Ocean, central Alps, Tectonics, 28, 2009.

https://doi.org/10.5194/se-2020-44
Preprint. Discussion started: 29 April 2020

Willett, S. D., and Schlunegger, F.: The last phase of deposition in the Swiss Molasse Basin: From foredeep to negative-alpha basin, Basin Research, 22, 623-639, 2010.

Zweigel, J., Aigner, T., and Luterbacher, H.: Eustatic versus tectonic controls on Alpine foreland basin fill: sequence stratigraphy and subsidence analysis in the SE German Molasse, Geological Society, London, Special Publications, 134, 299-323, 1998.

https://doi.org/10.5194/se-2020-44
Preprint. Discussion started: 29 April 2020

Solid Earth Discussions
Open Access
EGU

Table 1

Sample Name	Unit of SMB	Latitude	Longitude	Elevation (M)	Dep. Age (Ma)	+/- (Ma)	U-Pb	Geochem	Loc. of Analysis
Thun, CH									
OA13-SFB03	LFM I	46.789815	7.711673	740	27	0.5	x		UT
OA13-SFB04	LFM I	46.783249	7.730281	840	26	0.5	x		UT
10SMB06	LFM II	46.77989	7.6556	689	23	2.5	x		KU
10SMB07	UFM	46.81503	7.65013	689	18	3	x		KU
Lucerne, CH									
09-SFB-38	UFM	47.14054	8.19664	461	13.5	1	x	x	UT
09-SFB-11	UFM	47.10245	8.35003	420	14	1	x		KU
09-SFB-07	UFM	47.0569	8.24923	478	15.5	1	x		UT
09-SFB-12	UFM	47.10245	8.35003	420	16	1	x		UT
09-SFB-14	UMM	47.06692	8.32032	476	17.5	1	x	x	UT
09-SFB-49	UMM	47.02051	8.2403	676	19	1	x	x	UT
09-SFB-29	UMM	47.06442	8.32369	498	19	1	x		KU
09-SFB-05	UMM	47.05639	8.31036	398	20	1	x		UT
09-SFB-33	LFM IIb	47.05681	8.34139	503	21	1	x	x	UT and KU
09-SFB-08	LFM IIb	47.04211	8.32706	442	21.5	1	x		UT
09-SFB-13	LFM IIb	47.0565	8.38408	547	21.5	1	x		KU
09-SFB-21	LFM IIa	47.03422	8.35363	436	22.5	1	x	x	UT
09-SFB-45	LFM I	47.041	8.4614	1332	27	1	x	x	UT
09-SFB-10b	LMM	47.00933	8.29391	615	32	1	x		KU
09-SFB-43	NHF	46.87763	8.66345	496	35	3	x	x	
09-SFB-02	NHF	46.89991	8.6262	461	35	3	x		KU
Bregenz, AT									
10SMB09	UFM	47.53763	9.76789	609	15	2	x		UT
10SMB10	UMM	47.50168	9.79451	622	19	2	x		UT and KU
10SMB11	LFM II	47.48016	9.76906	442	22	2	x		UT
10SMB12	LMM	47.44407	9.78484	442	31	1	x		UT

Table 1. Sample Information. Depositional age errors are based on: Lucerne Section- Schlunegger et al. (1997a); Thun Section- Schlunegger et al. (1993; 1996); Bregenz Section- Oberhauser (1994), Kempf et al. (1999), and Schaad et al. (1992). 'X' in 'U-Pb' and 'Geochem' columns indicate data available for that sample. Final column indicates if samples were analyzed at either the University of Kansas (KU) or the University of Texas at Austin (UT). Errors for depositional ages are discussed in Section 3. Corresponding methods are found in the Section 4.

https://doi.org/10.5194/se-2020-44
Preprint. Discussion started: 29 April 2020

Solid Earth
Discussions
Open Access

Figure 1

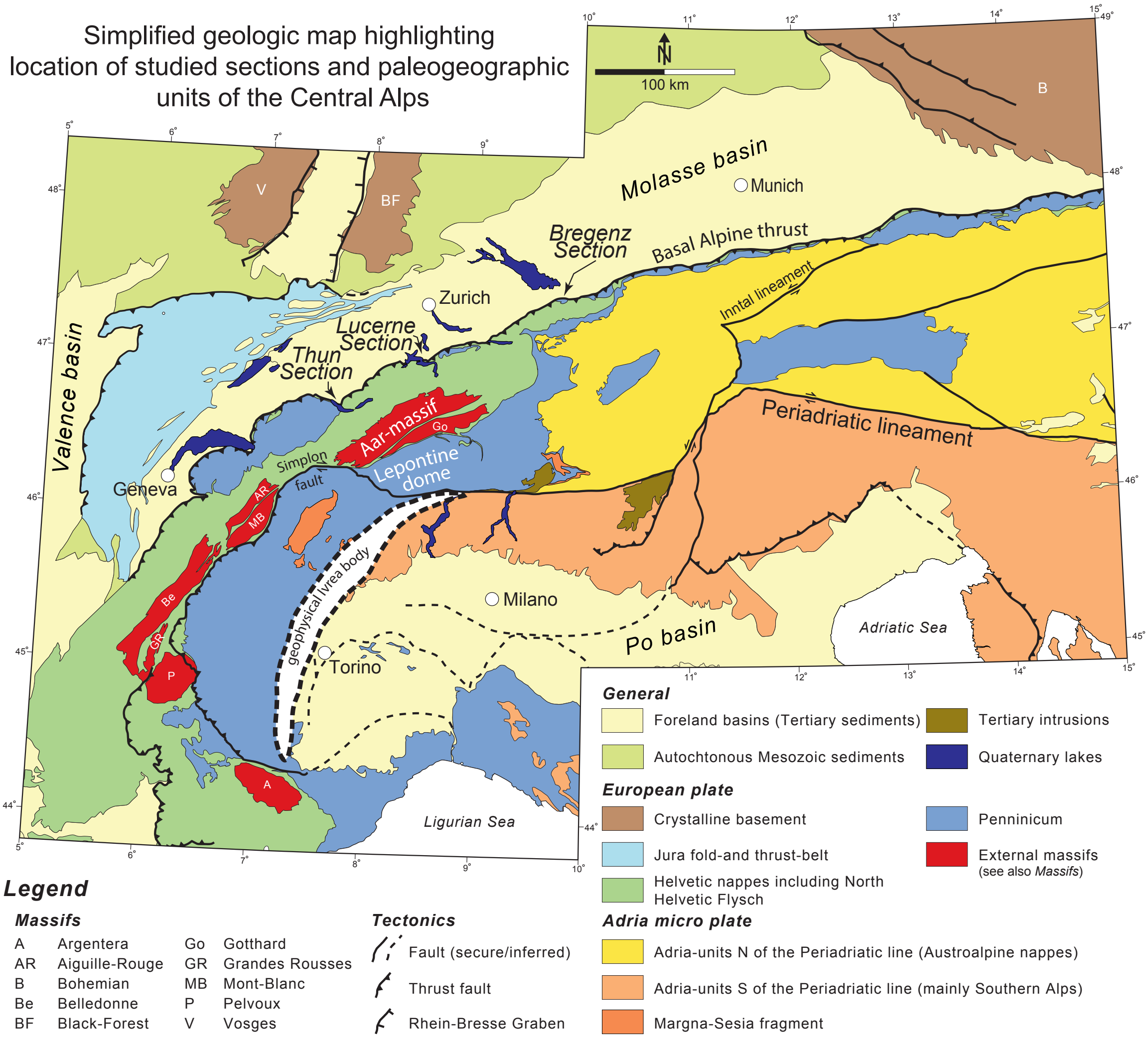

Figure 1. Geologic map of the Central Alps and Swiss Molasse Basin highlighting geologic features and paleogeographic units discussed in the text (map is adapted from Garefalakis and Schlunegger (2019) and based on: Froitzheim et al. (1996), Schmid et al. (2004), Handy et al. (2010), and Kissling and Schlunegger (2018). Locations are shown for the Lucerne Section, Thun Section, and Bregenz Section that are highlighted in Figures 3a, 3b, and 3c, respectively.

https://doi.org/10.5194/se-2020-44
Preprint. Discussion started: 29 April 2020

Solid Earth Discussions

Figure 2

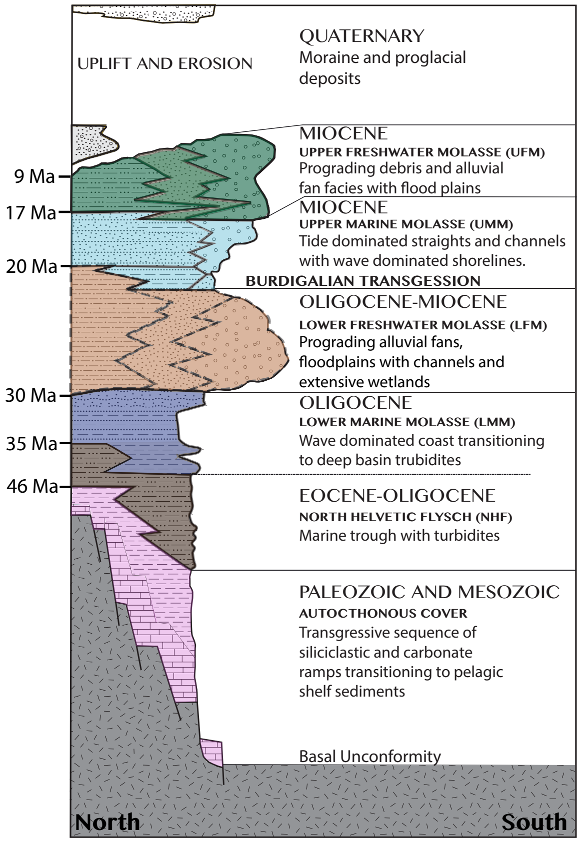

Figure 2. Generalized stratigraphy of the Molasse Basin. Modified from Miller (2009) and (Keller, 2000).

https://doi.org/10.5194/se-2020-44
Preprint. Discussion started: 29 April 2020

Solid Earth
Discussions

Figure 3

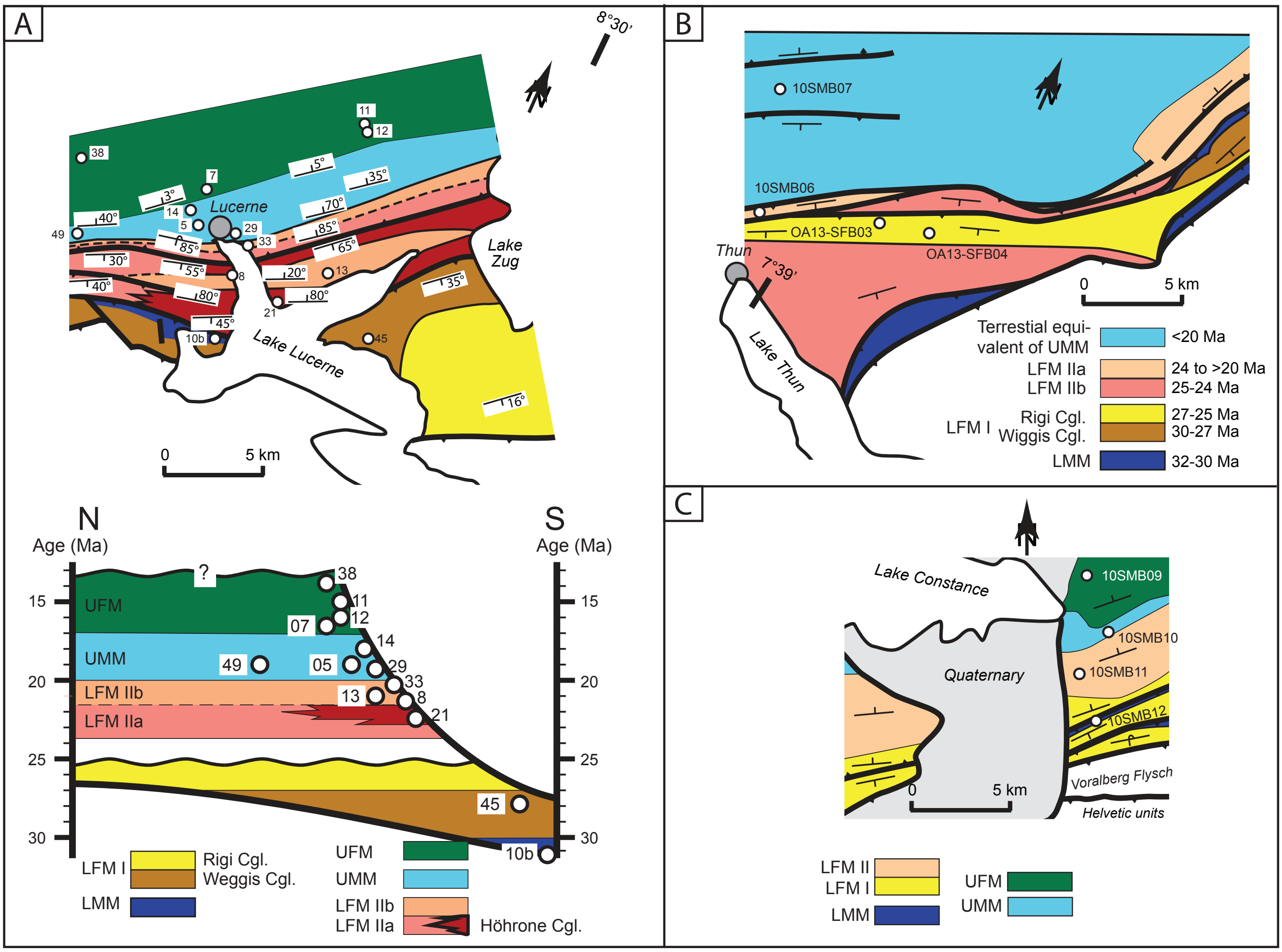

Figure 3. Stratigraphic units and sample locations of the three sampled sections A) Lucerne Section: geologic map and cross section modified from (Schlunegger et al., 1997a). In both the map and the simplified cross section, sample numbers are only the last two digits of the sample numbers from Table 1. B) Thun Section: geologic map modified from Schlunegger et al. (1993; 1996). C) Bregenz Section: geologic map simplified from Oberhauser, (1994), Kempf et al., (1999), and Schaad et al. (1992).

https://doi.org/10.5194/se-2020-44
Preprint. Discussion started: 29 April 2020

Solid Earth
Discussions

Figure 4

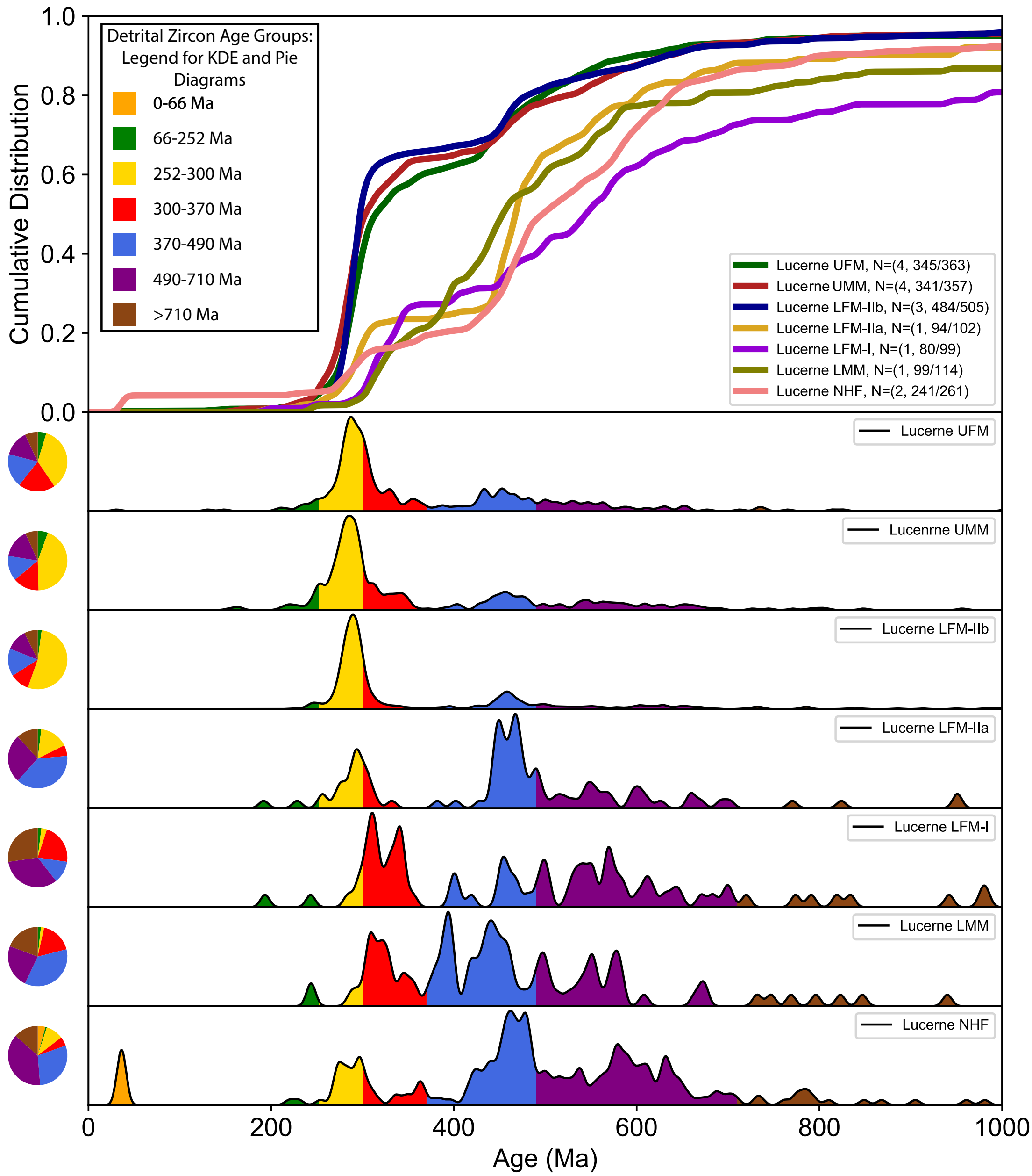

Figure 4. Detrital zircon U-Pb age data from the Lucerne Section (locations of samples depicted in Figure 3a) plotted as Kernel Density Estimations (KDE; Bandwidth set to 10), a Cumulative Distribution Plot (CDP), and as pie diagrams. Colored bars in the KDE and colored wedges in the pie diagrams show the relative abundance of age groups discussed in Section 5. Samples associated with each unit are referenced in Table 1. Plot only shows ages from 0-1000 Ma; however, a small number of older ages were analyzed and that data can be found in Supplemental File 1. N= (Number of samples, number of ages depicted/ total number of total ages).

https://doi.org/10.5194/se-2020-44
Preprint. Discussion started: 29 April 2020

Solid Earth
Discussions
Open Access
EGU

Figure 5

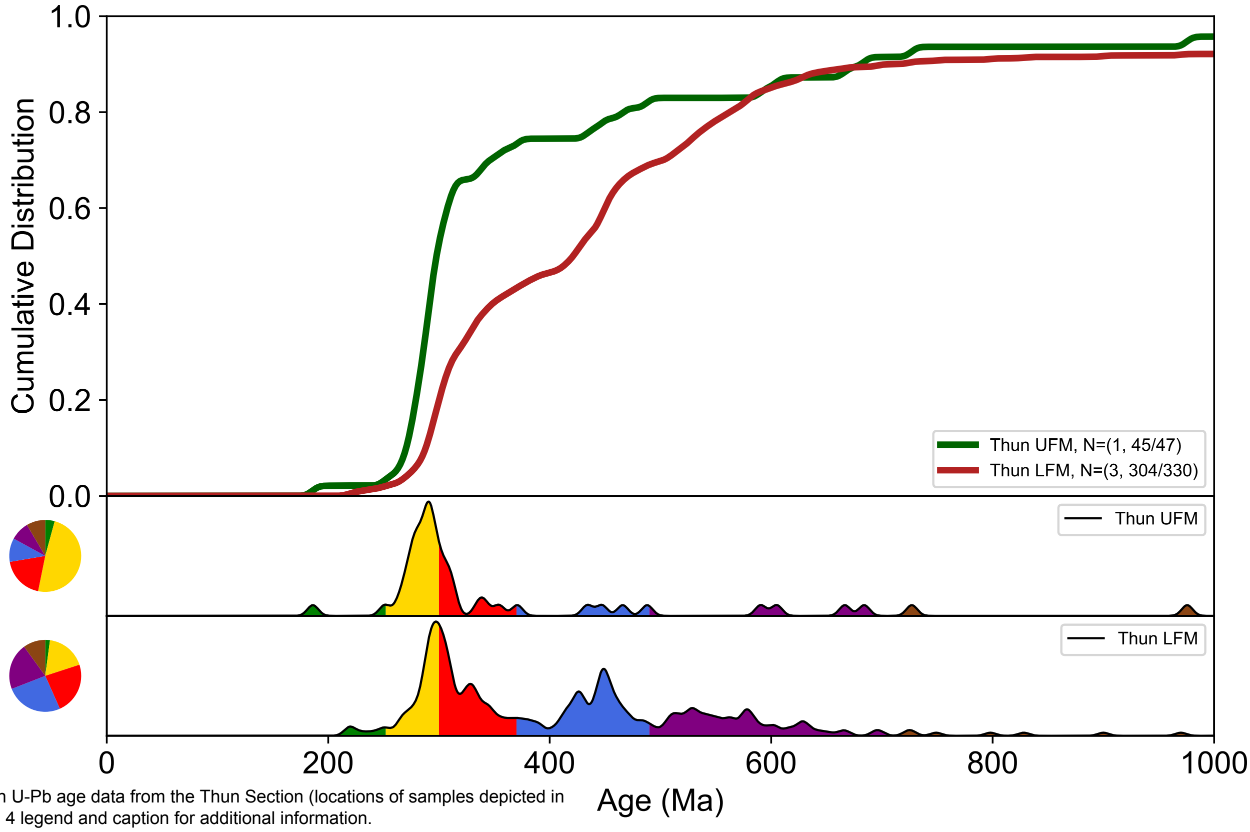

Figure 5. Detrital zircon U-Pb age data from the Thun Section (locations of samples depicted in Figure 3b). See Figure 4 legend and caption for additional information.

https://doi.org/10.5194/se-2020-44
Preprint. Discussion started: 29 April 2020

Solid Earth
Discussions
Open Access
EGU

Figure 6

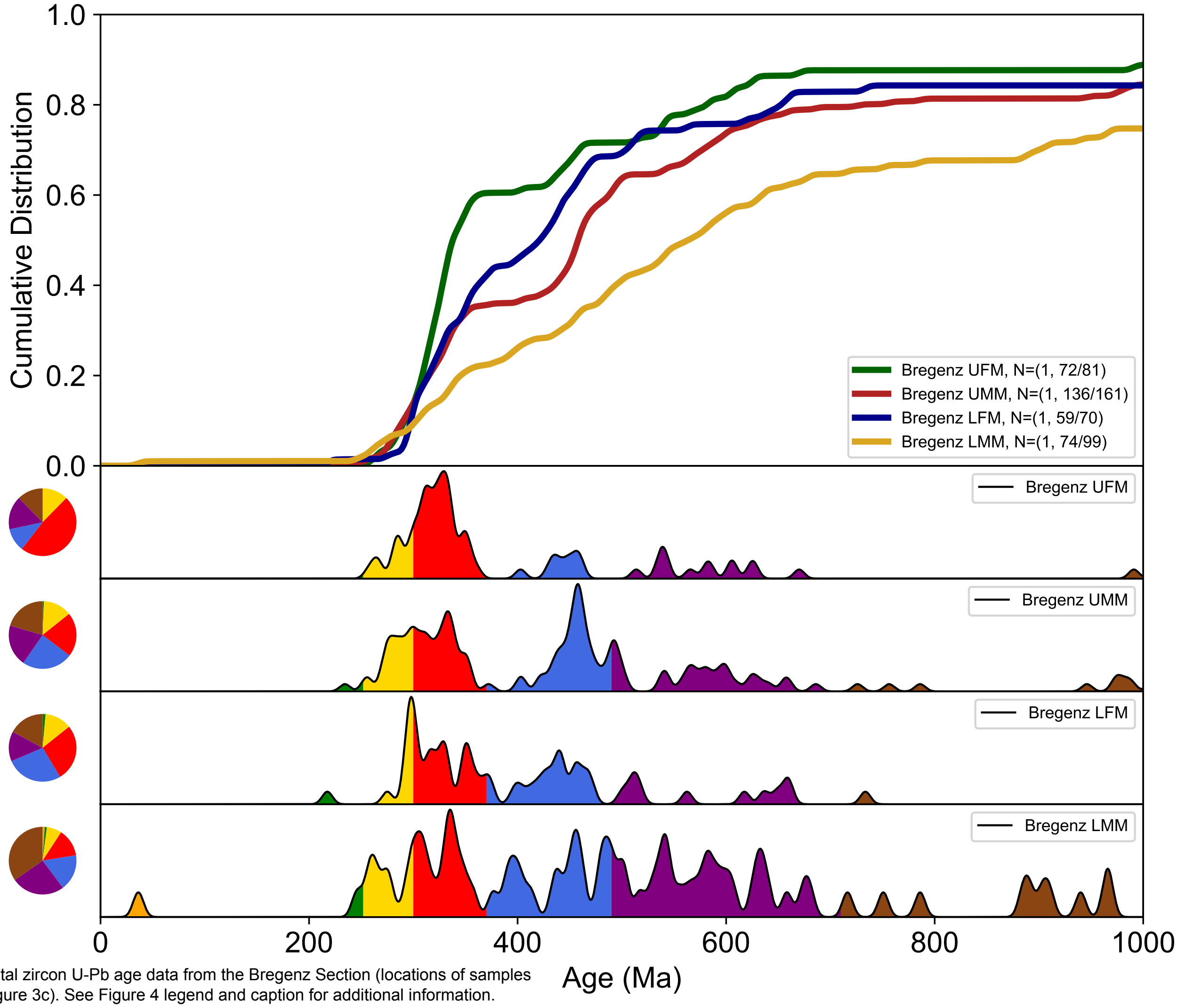

Figure 6. Detrital zircon U-Pb age data from the Bregenz Section (locations of samples depicted in Figure 3c). See Figure 4 legend and caption for additional information.

https://doi.org/10.5194/se-2020-44
Preprint. Discussion started: 29 April 2020

Solid Earth
Discussions

Figure 7

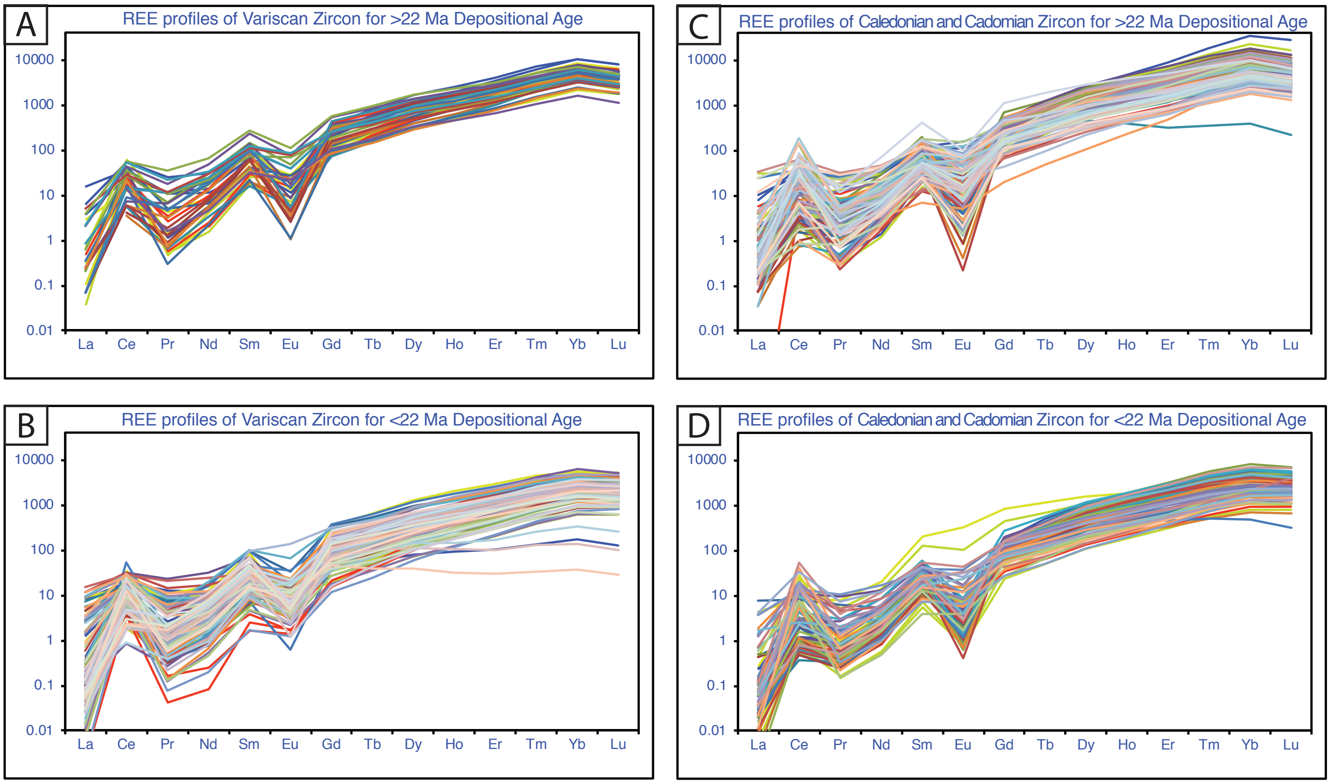

Figure 7. Detrital zircon Rare Earth Element (REE) spider diagram for samples collected from the Lucerne Section. (A) Variscan U-Pb ages and REE data for samples younger than a 22 Ma depositional age and (B) older than a 22 Ma depositional age. (C) Caledonian and Cadomian U-Pb ages and REE data for samples younger than a 22 Ma depositional age and (D) older than a 22 Ma depositional age. For plots A and C the geochemical data is drawn from samples SFB33 (21 Ma), SFB49 (19Ma). SFB14 (17.5 Ma), and SFB38 (13.5 Ma). For B and D the geochemical data is drawn from samples SFB21 (22.5 Ma) and SFB45 (27 Ma). The data suggest that detrital zircons from all three recent orogenic cycles record primarily grains that are magmatic in origin (Belousova et al., 2002; Hoskin and Ireland, 2000), with little evidence of metamorphic/metasomatic grains. Data can be found in Supplemental File 2.

https://doi.org/10.5194/se-2020-44
Preprint. Discussion started: 29 April 2020

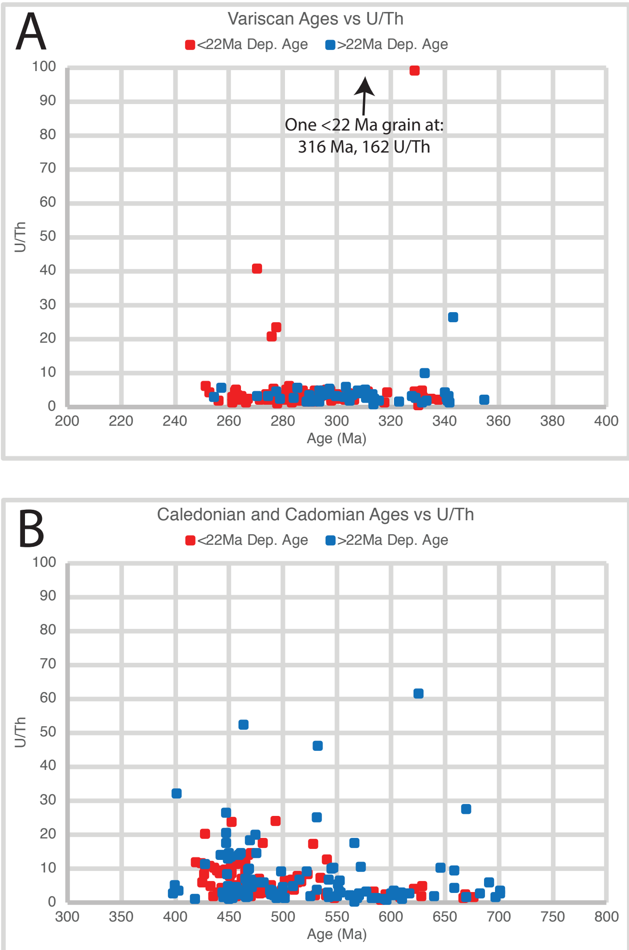

Figure 8

Figure 8. Age vs U/Th comparison for detrital zircon grains with depositional ages older than 22 Ma and younger than 22 Ma. A) Variscan aged grains, B) Caledonian and Cadomian age grains. Although not definitive, grains with elevated U/Th (or low Th/U; e.g. Rubatto et al. 2002) have a higher likelihood of being metamorphic in origin. There are few Variscan grains with elevated U/Th from both the pre- and post-22 Ma depositional ages, suggesting little input of metamorphic sources for these ages. There are a large number of Caledonian and a handful of Cadomian grains with elevated U/Th from both the pre- and post-22 Ma depositional ages, indicating metamorphic sources for these age grains are prevalent.

https://doi.org/10.5194/se-2020-44
Preprint. Discussion started: 29 April 2020

Solid Earth
Discussions
Open Access

Figure 9

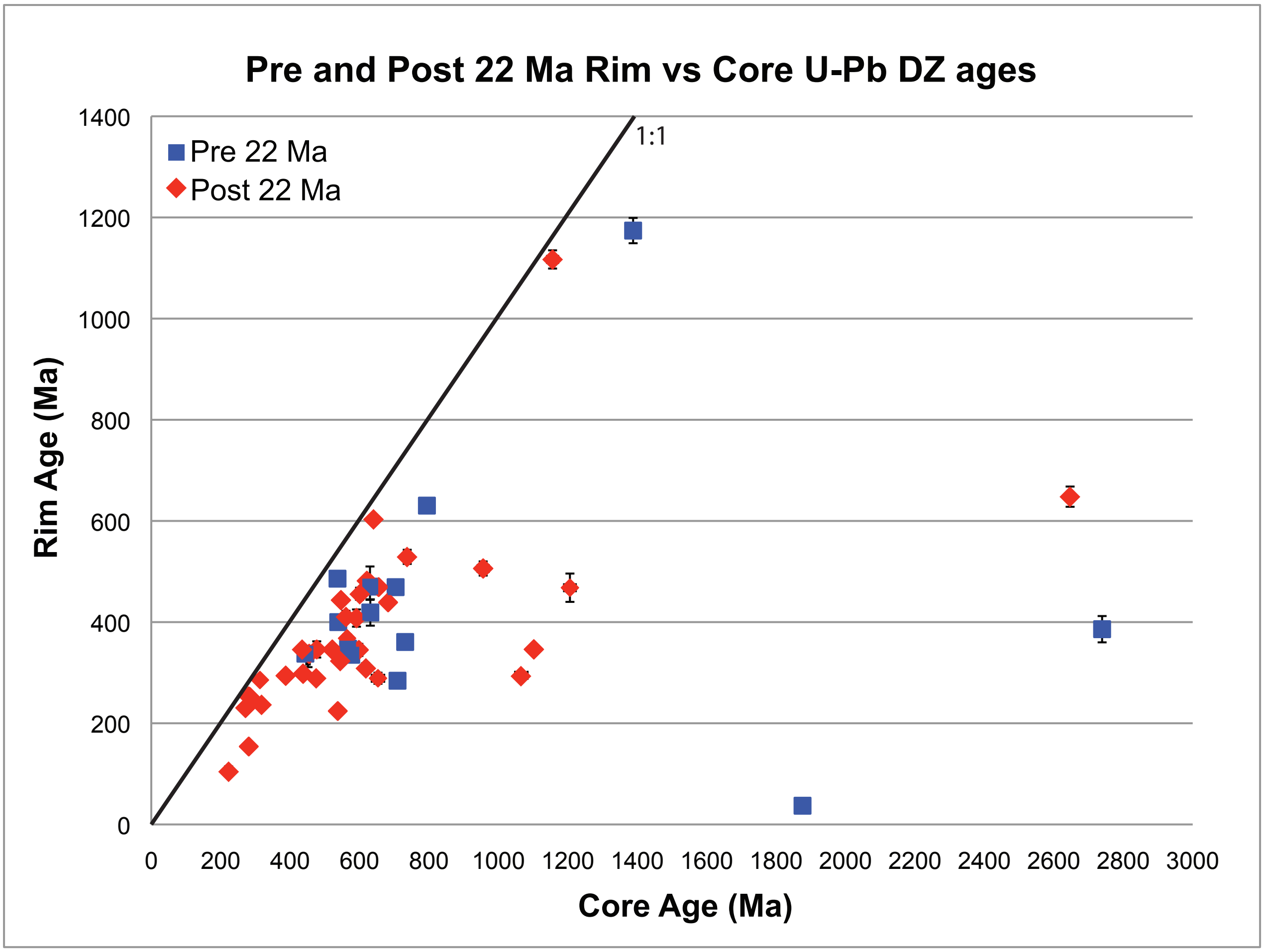

Figure 9. Rim vs core ages for detrital zircon grains from samples with depositional ages older than 22 Ma and younger than 22 Ma from the Lucerne Section. Prior to the 22 Ma transition in source area there is a minor number of Variscan rims on Cadomian and Caledonian cores. In samples younger than 22 Ma there is a noticeable increase in Variscan rims on Caledonian, Cadomian, and Proterozoic cores. Error bars are 2 sigma non-propagated errors.

https://doi.org/10.5194/se-2020-44
Preprint. Discussion started: 29 April 2020

Solid Earth
Discussions
Open Access
EGU

Figure 10

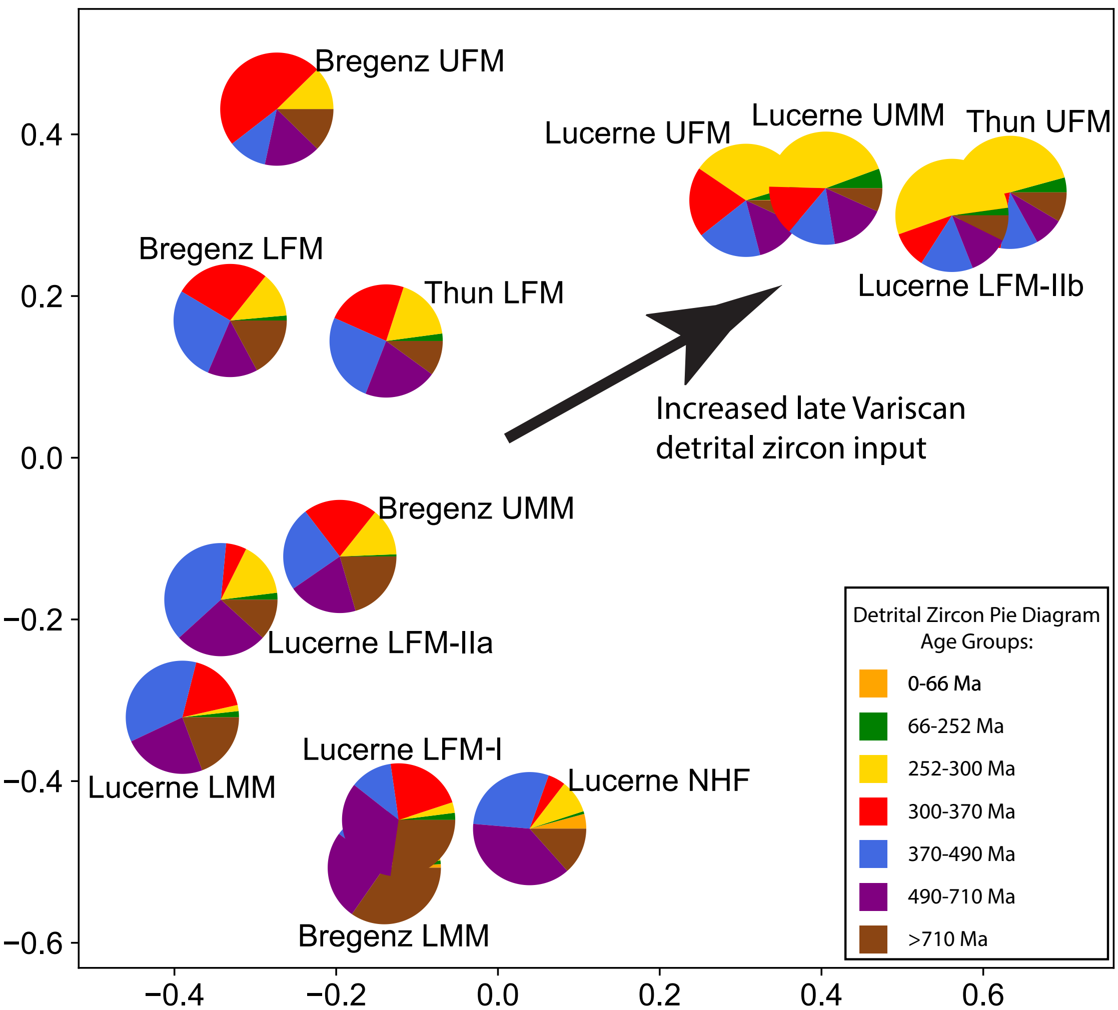

Figure 10. Multidimensional Scaling Plot (MDS) of detrital zircon U-Pb ages for all units from the Molasse Basin. The MDS plot was produced with the DetritalPy software of Sharman et al. (2018b) and is based on methods outlined by Vermeesch (2018). Pie diagram colors correspond to age groups from Figure 4 and ages discussed in Section 4.

https://doi.org/10.5194/se-2020-44
Preprint. Discussion started: 29 April 2020

Solid Earth Discussions
Open Access
EGU

Figure 11

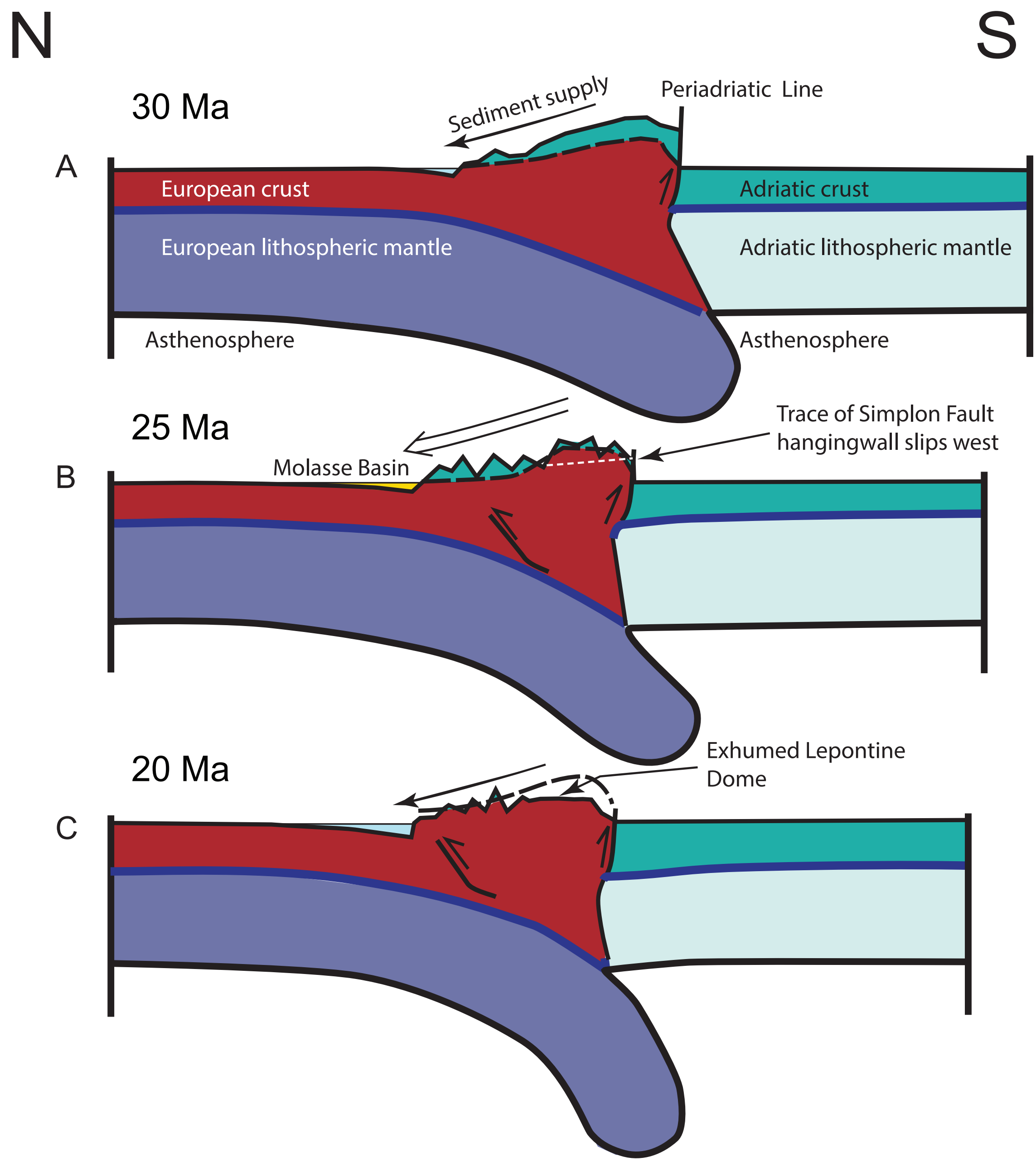

Figure 11. Schematic cross-section through the central Alps of Switzerland, illustrating the development of the Alpine relief and the topography through time. A) 30 Ma-25 Ma: Slab breakoff resulted in backthrusting along the Periadriatic fault and in the growth of the Alpine topography. The erosional hinterland was mainly made up of the Austroalpine cover nappes (Adriatic plate) and Penninic sedimentary rocks at the orogen front. B) 25 Ma: Ongoing surface erosion resulted in the formation of an Alpine-type landscape with valleys and mountains. First dissection into the crystalline core of the European continental plate was registered by the first arrival of Penninc crystalline material in the foreland basin sometime between 25 and 22 Ma, depending on the location within the basin. 22 Ma was also the time when sediment discharge to the Molasse was highest. Tectonic exhumation through slip along the Simplon fault started to occur at the highest rates. C) 20 Ma: Tectonic exhumation along the Simplon fault resulted in widespread exposure of high-grade rocks, in a shift in the clast suites of the conglomerates and in a change in the detrital zircon age signatures. Faulting along the detachment fault most likely subdued the topography in the hinterland. As a result, sediment flux to the Molasse basin decreased, and the basin became underfilled and was occupied by the peripheral sea of the Upper Marine Molasse. (Figures based on restored sections by Schlunegger and Kissling, 2015).